

Kaolinite deposition from moving suspensions: The roles of flocculation, salinity, suspended sediment concentration and flow velocity/bed shear

JUERGEN SCHIEBER* , ZHIYANG LI†, ZALMAI YAWAR*, XIAOMENG CAO‡ , THOMAS ASHLEY§ and RYAN WILSON¶

*Department of Geological Sciences, Indiana University, 1001 E 10th Str, Bloomington, IN, 47405, USA (E-mail: jschiebe@indiana.edu)

†Department of Geology, Colorado College, Colorado Springs, CO, 80903, USA

‡Pilot National Laboratory for Marine Science and Technology (Qingdao), 168 Wenhai Middle Rd, Aoshanwei, Jimo District, Qingdao, Shandong, 266237, China

§Civil & Environmental Engineering, Virginia Tech, Patton Hall 221D (0105), 750 Drillfield Drive, Blacksburg, VA, 24061, USA

¶Chevron Technology Center, 1400 Smith St, Houston, TX, 77002, USA

Associate Editor – Lauren Birgenheier

ABSTRACT

Understanding how mud moves and deposits is essential for conceptualizing the dynamic nature of surface environments and their ancient counterparts. Experimental study has largely been pursued by civil engineers, using kaolinite as an active ingredient. Yet, applying their data to the physical comprehension of mudstone sedimentology is hampered by multiple flume configurations between labs, and data sets tailored to specific engineering needs. The need for a better grasp of underlying processes is acute, given recent flume studies that show that moving suspensions form large bedload floccules, migrating floccule ripples and bed accretion under currents capable of moving sand grains. To advance mudstone sedimentology, integrated study of suspended sediment concentration, salinity and bed shear stress on the deposition of floccules is crucial. Described here is a set of tightly controlled experiments that explored suspended sediment concentrations from 70 to 900 mg/l, freshwater, brackish and marine salinities, flow velocities in the 5 to 50 cm/s range (equivalent to 0.01 to 0.58 Pa bed shear), measured the size of in-flow and bedload floccules, and the critical velocity of sedimentation that marks the onset of sustained bedload accumulation. The critical velocity of sedimentation of kaolinite clays is in the 26 to 28 cm/s flow velocity range (0.22 to 0.25 Pa), appears insensitive to a wide range of suspended sediment concentrations and salinities, and coincides with the formation of sand-size bedload floccules. Further decrease of flow velocity/bed shear stress is accompanied by a steady increase in the size of bedload floccules. Large bedload floccules appear to form in the high-shear basal part of the flow, a phenomenon requiring further investigation. Better understanding of the mechanisms that facilitate mud deposition from moving suspensions is critical for more realistic assessments of the depositional conditions of mud and mudstones, as well as for refining predictive models for the flux of fine-grained sediments across the Earth's surface.

Keywords Depositional environment, evaporite, Gale Crater, geochemistry, Mars, mudstone, provenance, sequence stratigraphy.

INTRODUCTION

Although at first glance deceptively uninteresting looking sediments, muds are the most abundant sediment type on the surface of modern Earth, and mudstones are the dominant sedimentary rock type from the Archean onward (Potter *et al.*, 2005). As Sorby (1908) so eloquently put it: “much of the history of our rocks appears to be written in this language”, and thus a quantitative understanding of mudstone depositional processes has to be a key objective of contemporary research in sedimentary geology. It may well be a complex and difficult undertaking (Berlamont *et al.*, 1993; Schieber *et al.*, 2007), but mudstones are the integrative matrix of the sedimentary rock record and understanding how they work is no longer optional. In order to get there requires going beyond the established knowledge base, and to do experimental work that provides ‘rates and processes’ in a form that facilitates sedimentological research of modern as well as ancient systems.

Flocculation, a phenomenon where multiple parameters such as grain-size distribution, mineral properties, salinity and organic content converge in rather complex ways to produce aggregates – floccules – that are much larger than their component particles, is a core issue in mud sedimentation and mudstone sedimentology. It is an important process that governs the transport and deposition of mud in a wide range of depositional environments, including rivers and associated floodplains, coastal environments (for example, estuarine and prodelta) and continental shelves (Kranck, 1973; Sternberg *et al.*, 1999; Hill *et al.*, 2001; McAnally & Mehta, 2002; Safak *et al.*, 2013; Shchepetkina *et al.*, 2018; Lamb *et al.*, 2020). Whereas its main role has long been thought of as simply increasing the (passive) effective settling velocity of mud, the research presented here aims to document that this is too narrow of a perspective.

Because flocculation plays such a key role in the transport and deposition of muds (McCave, 1975; Syvitski *et al.*, 1995; Schieber *et al.*, 2007) and their adsorbed constituents (organic matter, nutrients, contaminants), the factors that govern flocculation have been studied extensively across a range of disciplines, such as hydraulic engineering, environmental engineering and oceanography (Patterson, 1985; Burban *et al.*, 1989; Mehta *et al.*, 1989; Manning & Dyer, 1999; Haralampides *et al.*, 2003). In

natural settings, main constituents of floccules include sub-micron to micron-size mineral grains (clays, quartz, etc.), as well as organic matter and abundant water (Safak *et al.*, 2013). They are held together by van der Waals electrostatic forces (Kranck, 1973; Mehta *et al.*, 1989; Syvitski *et al.*, 1995) as well as by organic matter (Furukawa *et al.*, 2014). The latter topic is an area of active research (Asmala *et al.*, 2014; Ye *et al.*, 2020) and likely will have a significant impact on future understanding of mudstone sedimentology.

In moving suspensions, continuous particle aggregation and aggregate breakup arises from the complex interplay of fluid shear, suspended sediment concentration and salinity (Burban *et al.*, 1989; Lick *et al.*, 1993; Manning & Dyer, 1999; Haralampides *et al.*, 2003; Xu *et al.*, 2008; Mietta *et al.*, 2009; Safak *et al.*, 2013). For example, increasing turbidity (measured with a calibrated turbidity sensor as ‘suspended sediment concentration’, or SSC, in mg/l) at low shear levels is thought to produce constructive particle collision and floccule growth, whereas above a critical shear stress increasing turbidity may lead to the disaggregation of floccules (Milligan & Hill, 1998; Manning & Dyer, 1999; Hill *et al.*, 2001; Haralampides *et al.*, 2003; Stone & Krishnappan, 2003; McCool & Parsons, 2004; Safak *et al.*, 2013). The influence of salinity on floccule size remains controversial. Although some studies have documented an increase in floccule size with increasing salinity (van Leussen, 1999), other studies have found the opposite relationship to be true – decreasing floccule size with increasing salinity (Burt, 1986; Burban *et al.*, 1989). To independently establish the effect of each controlling factor on floccule size and transport mode is challenging because multiple physical properties are closely associated or interdependent with one another (Mietta *et al.*, 2009).

From a sedimentological perspective, there are two types of floccules to consider when studying transport and deposition of muds: (i) in-flow floccules that are present within moving suspensions (Hill *et al.*, 2001; McCave & Hall, 2006); and (ii) floccules that presumably travel as bedload at the base of turbid flows. Whereas the former have received considerable attention (Winterwerp & van Kesteren, 2004), comparatively little is known about bedload floccules that nonetheless seem essential for the accretion of mud beds (Schieber *et al.*, 2007). The research presented here is aimed at improving

the understanding of the influence of first order parameters (SSC, salinity, flow velocity/shear) on floccule generation and growth in an organic-free setting, in order to lay the physical foundation for future studies where organic matter will be included. It builds on earlier work (Schieber *et al.*, 2007; Schieber, 2011) that documented the presence of large bedload floccules at the base of muddy flows. The undisputable presence of these floccules is at odds with conventional wisdom because the assumption always was that floccules should disintegrate at the base of these flows owing to maximum shear rates (Einstein & Li, 1956; Schlichting, 1979; Mehta & Lott, 1987; McCave & Hall, 2006). In the present study, the ubiquitous observation of small in-flow floccules in flows that at the same time show large bedload floccules once active bedload transfer commences, is a phenomenon that can be described as the 'basal shear conundrum'. Whereas it seems inescapable that the large floccules do indeed form in that part of the flow that experiences the highest shear rates, what the underlying mechanism might be requires further investigation with still to be designed instrumentation. Irrespective of the eventual solution to the 'basal shear conundrum', some plausible working hypotheses are proposed in the *Discussion* section of this paper. Mud transport and deposition by bedload floccules is at the heart of a paradigm shift in the sedimentology community with regard to transport and deposition of mud in both modern and ancient mud-dominated systems (Macquaker & Bohacs, 2007; Aplin & Macquaker, 2011; Ghadeer & Macquaker, 2011; Plint *et al.*, 2012; Trabuchon-Alexandre *et al.*, 2012; Chang & Flemming, 2013; Steel & Milliken, 2013; Lazar *et al.*, 2015; Newport *et al.*, 2016; Schieber, 2016; Schieber *et al.*, 2019; Smith *et al.*, 2019; Li *et al.*, 2021).

Given that moving muddy suspensions demonstrably form bedload floccules over a wide range of experimental conditions (Schieber, 2011), a comprehensive examination of how the interaction of suspended sediment concentration, salinity and bed shear stress influence the formation and preservation of these floccules is long overdue. Experimental studies of clay behaviour in sedimentation processes, be they by civil engineers or sedimentologists (Mehta & Partheniades, 1979; Baas & Best, 2002; Schieber *et al.*, 2007) in most cases use kaolinite because of its ready availability and an abundance of published studies. The focus of this study is a multiparameter

investigation of kaolinite flocculation in flume experiments that produce sediment accumulation associated with bedload transport of flocculated clays, with particular attention paid to the critical velocity of sedimentation and rates of bedload transfer.

For experimental studies of mudstone sedimentology, the critical velocity of sedimentation (CVS) is a convenient measure of whether or not a mud bed will accumulate in the course of an experiment. The CVS is that flow velocity below which flocculated muds accumulate at the base of the flow, form ripples and build up sediment (Schieber *et al.*, 2007; Schieber, 2011). It relates to the critical shear stress for deposition (Berlamont *et al.*, 1993), a value of bed shear stress below which all sediment will eventually deposit from suspension. Whereas in the annular flumes used by Berlamont *et al.* (1993) bed shear stress is very easy to quantify, in the racetrack flumes used for the described kaolinite experiments flow velocity is a more easily recorded descriptor of fluid motion. Given that, in turbulent flows, flow velocity has a quadratic relationship to bed shear stress (Clauser, 1954), the critical velocity of sedimentation is used here as an analogue measure to describe the flow velocity below which all sediment will eventually deposit from suspension. Details on measuring shear stress are provided in the *Methods* section.

Results from this study show that, for kaolinite at least, the critical velocity of sedimentation (or more universally its bed shear stress equivalent) is largely independent of suspended sediment concentration and salinity, and equates to approximately 27 cm/s at 5 cm flow depth (equivalent to a bed shear stress of *ca* 0.23 Pa). Future expansion of these experimental protocols to other clay minerals and mineral mixtures will provide a better understanding of the processes and factors that have a bearing on the critical shear stress of deposition for natural muds and will facilitate a more quantitative understanding of the depositional parameters needed for the accumulation of fine-grained sediments and sedimentary rocks. Whereas the experiments described here were conducted with pure kaolinite clay, an end-member mud composition, natural muds are a mixture of clay and silt, and the addition of silt to clay suspensions has an influence on sedimentation behaviour and the textural outcome of mud deposition (Yawar & Schieber, 2017). Nonetheless, because clays and silt tend to segregate during transport (Yawar & Schieber, 2017),

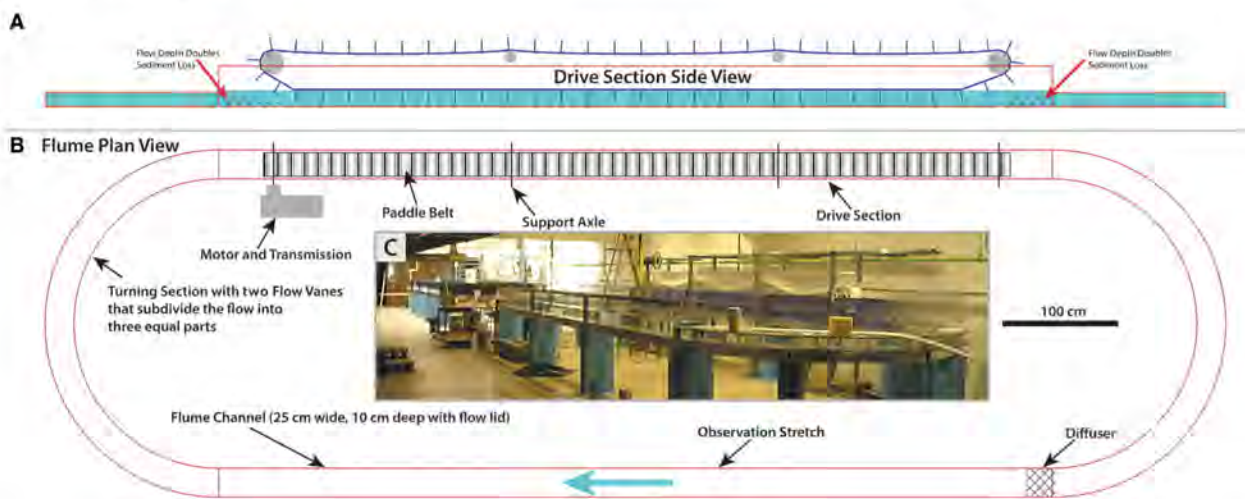


Fig. 1. Schematic sketches of the racetrack flume used in the described experiments. (A) Sideview of the drive section showing the paddle belt (water fill in blue). Red arrows point to areas of sediment accumulation where (at left) change of flow depth (from 5 to ca 14 cm) and reduction of turbulence results in sediment deposition. (B) Plan view of flume, showing channel configuration and location of design elements. (C) A photograph of the flume. Because of the need for boundary layer development after the flow leaves the diffuser, observations on floccule and bedform (ripples) development were restricted to the downstream 5 m of the observation stretch.

studying the behaviour of end member compositions (such as pure clay) provides critical insights into the behaviour of muddy flows.

METHODS

The racetrack flume used for the described experiments (Fig. 1) is of the same design and dimensions as reported in previous publications (Schieber *et al.*, 2007; Schieber & Southard, 2009; Schieber, 2011; Yawar & Schieber, 2017). There is a fixed surface at the bottom (channel base) and top (flow lid) of the flow. The flow lid is added to maintain uniform bed shear across the length of the flume channel. In regular flumes this is achieved by tilting the flume channel to compensate for friction loss, but in racetrack flumes this option is not available. Adding a flow lid converts the flow from open channel to flow through a rectangular duct and ensures uniform distribution of bed shear. The pressure drop along this duct was used to calculate the averaged shear stress on the duct surface, a number that also represents the bed shear stress. The distance between the flume bottom (channel base) and the flow lid was 10 cm, and the effective flow depth is half that distance (5 cm). The turning sections contain two parallel vanes to reduce secondary circulations. A

diffuser was placed at the upstream end of the observation section.

Across the entire flow velocity range used in these experiments (5 to 50 cm/s), the Reynolds number calculated for a rectangular duct is in the fully turbulent range (R_e ca 7119 to 71 190; see Appendix S1). Given the smooth boundary presented by the flume bottom, a standard turbulent boundary layer (Middleton & Southard, 1984) is assumed. The viscous sublayer is on the order of a millimetre or less in thickness and thus the effective flow depth is at least an order of magnitude thicker. Under fully turbulent conditions, the suspended material should be distributed evenly across the height of the duct (10 cm). This supposition is confirmed by measurements of SSC from bottom to top (0 to 10 cm), that did not show discernible gradients.

The kaolinite clay used in the experiments, Acti-Min SA1 kaolin, was donated to the IU Shale Research Lab by Active Minerals International LLC, Gordon, Georgia. Rietveld based X-ray diffraction (XRD) analysis of the shipment by Dr David Bish (IU Department of Chemistry), shows it to be composed of 95% kaolinite, 3.9% 2 M1 muscovite, 0.5% microcline and 0.5% quartz (see Appendix S2 for XRD data). The kaolinite is well-ordered, and the remaining components are residuals from the original material

that altered to form kaolinite, a common observation in other kaolinite deposits as well. The kaolinite was mixed with water and hydrated for at least 24 h, stirred in a blender for 10 min, and then the blended slurry was washed through a 63 µm sieve (to screen out any detrital sand grains) directly into the flume running at 50 cm/s velocity. The kaolinite feed (Fig. 2) has a grain-size distribution of 90% finer than 0.01 mm, 70% finer than 0.005 mm, and 50% finer than 0.002 mm. About 10 wt.% of the kaolinite feed are silt sized kaolinite particles larger than 0.01 mm (Fig. 2). Sediment concentrations ranging from 0.07 to 0.9 g/l were explored. Given that these concentrations are far below the 10 g/l that conventionally is considered the fluid mud threshold, the clay content of the examined flows

did not influence their turbulence structure (Baas & Best, 2002). Suspended sediment concentrations were monitored with a calibrated turbidity probe (OBS-3+; Campbell Scientific, Logan, UT, USA) positioned 5 cm above the flume base. Velocities were measured with a Marsh McBirney Flo-Mate 2000 electromagnetic velocity probe (Hach Company, Frederick, MD, USA) centred within the flow cross-section, and verified and cross-correlated with acoustic Doppler velocimeter (ADV) measurements (SonTek 10-MHz ADV; Xylem Inc., Washington, DC, USA) and rpm tracking of the drive motor. Velocity stepping was controlled with a programmable motor control system. Starting at 50 cm/s, the flow velocity was reduced stepwise in 5 cm/s increments, with 5 cm/s as the lowest tested velocity. Water

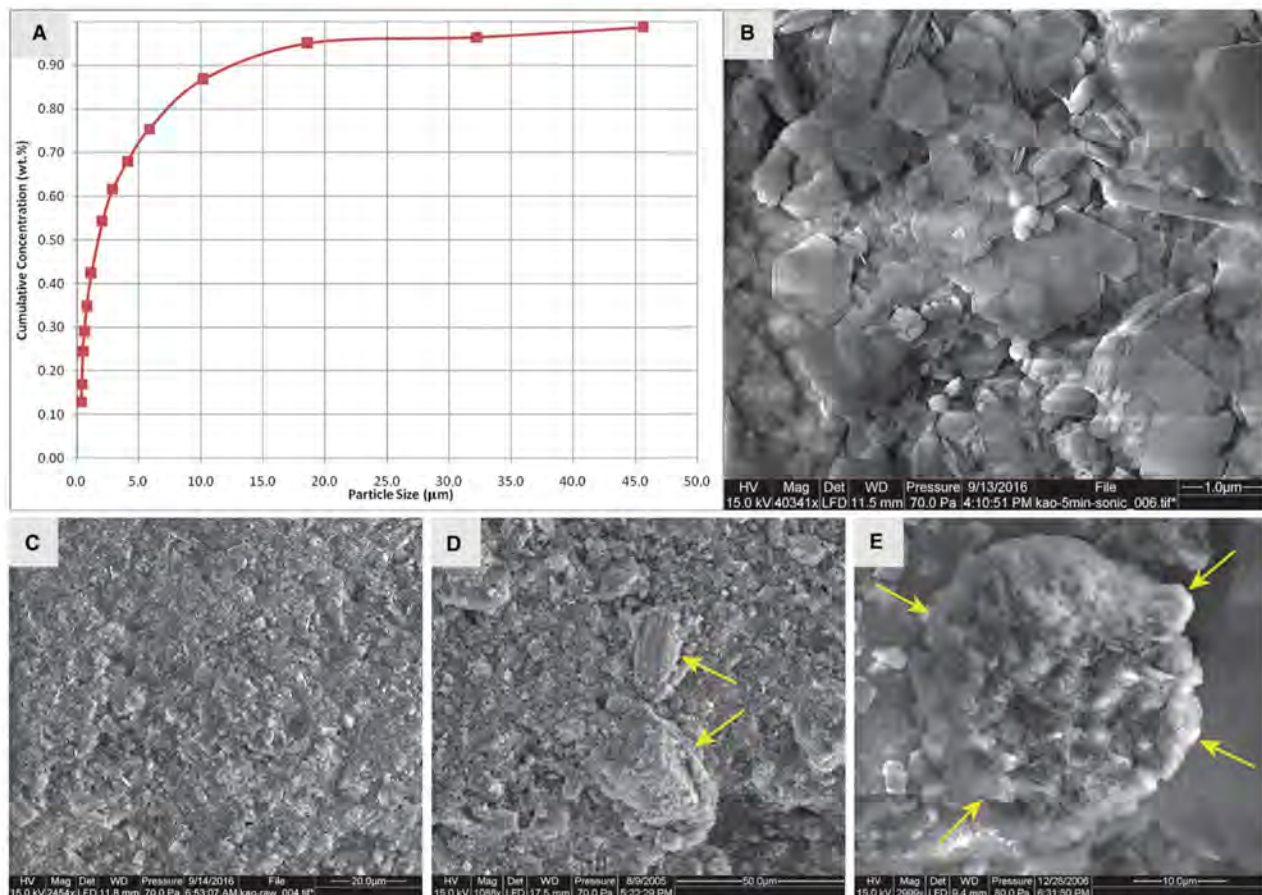


Fig. 2. (A) Grain-size distribution of the kaolinite used in experiments (determined by pipette method). Note that 70 wt.% of the material are smaller than 5 µm, and 10 wt.% are larger than 10 µm. (B) Scanning electron microscope (SEM) image of the dominant fine fraction, consisting of micron-size kaolinite platelets. (C) Overview SEM image of the kaolinite at lower magnification, showing larger particles buried in a finer matrix. (D) Closer view of these larger particles. They consist of larger stacks of kaolinite platelets and fragments of kaolinitic claystone. Yellow arrows point to coarse silt size kaolinite particles. (E) A rounded kaolinite floccule (in-flow), recovered from the flow in a kaolinite experiment. Yellow arrows mark outline of floccule.

samples to verify suspended sediment concentrations were collected at the start and end of each experiment and used to calibrate the readings from the optical backscatter sensor (OBS). Shear stress estimates were made by measuring the pressure drop along the observation stretch of the flume (Schieber *et al.*, 2013), and then balancing the down channel driving force against wall friction (a function of shear stress) to arrive at a value for the average shear stress. The derived shear stress values are in good agreement with values computed from ADV velocity profiles.

The suspension was too turbid to observe any details within the flow, but by shining strong lights from above through the flow it was possible to observe and film what was happening directly at the flume bottom. For observation of bedload floccules, a HD camera with a macro lens continuously recorded the flume bottom over a 28 by 16 mm area at a resolution of 6.85 µm per pixel. For each velocity step the film clips were subsampled for well-focused images that then were processed for contrast with ImageJ, and then visible and well-defined particles (silt grains and bedload floccules) were measured manually for size (dimension perpendicular to flow direction) with the ImageJ software package. Floccule measurements from multiple images were collated and evaluated statistically. In addition, time-lapse photography of the flume bottom was employed to record ripple formation and bed accretion in these experiments.

Violin plots were used to present the variation and distribution of particle size measured from HD film frames. A violin plot is a hybrid of a box plot incorporated with a kernel density plot, which simultaneously reflects the statistical features (maximum, minimum, median, and upper and lower quartiles) and frequency distribution of the data in more detail. For each violin plot, the vertical axis represents different values of the particle size, and the width in the horizontal direction represents the frequency of the occurrence of the particle size at this value. A wider part of the violin corresponds to a higher occurrence probability, and a thinner part indicates lower probability.

The experiments described in this paper were run multiple times for verification over a time period of ten years, using different sensors with increasingly (over time) better resolution. Through repetition, these experiments were

shown to be highly reproducible. Clays deposited in a given experiment can be re-suspended, and the experiment repeated with essentially identical results, and equally well experiments can be repeated with new charges of clay and produce the same results.

To better understand the size characteristics of 'in-flow' floccules (Fig. 2E), a floc camera system developed by Kyle Strom at Virginia Tech (Keyvani & Strom, 2013; Tran & Strom, 2017) was used. Suspended floccules were illuminated using a dimmable LED submerged inside a PVC enclosure with a flat plexiglass window and imaged using a FLIR Blackfly S machine vision camera (Teledyne FLIC LCC, Wilsonville, OR, USA) fitted with a 2× Mitutoyo objective (Mitutoyo Corporation, Kawasaki, Japan). Each measurement of median floccule size was computed from a total of 300 images acquired at a frequency of one image every 3 s. The camera setup produced 4000 × 3000 pixel greyscale images at a resolution of 0.95 µm per pixel from approximately 5 cm above the flume bottom.

Floccules were identified by an automated image processing algorithm implemented in Python using the scikit-image package (van der Walt *et al.*, 2014). Image processing included: (i) image smoothing using a wavelet denoiser; (ii) thresholding floccules from background; and (iii) subtracting static image features (stuck on dirt, etc.). Floccules were identified as contiguous regions below the threshold value. Out of focus floccules were identified according to the brightness gradient at the edge of the floccule using a procedure similar to one described by Keyvani & Strom (2013). Floccules with an equivalent diameter <5 µm were ignored because they cannot reliably be differentiated from noise at this scale. From these data median floccule sizes were computed.

Settling tube experiments were conducted to certify the settling properties of the used clay with regard to salinity and suspended sediment concentrations. This certification was done because depending on where a given kaolinite is mined and processed, its properties may differ from those that have been compiled in textbooks. In these settling experiments the kaolinite that was used in flume experiments was mixed with 1 l of the same water compositions (freshwater, 2.0% and 3.5% salinity) that were used in flume experiments, and the settling of these mixtures over time was recorded with a time-lapse camera.

EXPERIMENT DESIGN, OBSERVATIONS AND IMPLICATIONS

Although the behaviour of moving muddy suspensions has been studied in our lab for multiple materials for about 15 years (Schieber, 2011), earlier efforts were aimed at exploring basic properties and contrasts in behaviour (Schieber *et al.*, 2007, 2013; Schieber & Southard, 2009; Schieber, 2011), rather than systematic exploration of single materials/minerals and the controls on their specific sedimentation properties. The data presented here are the result of a systematic examination of the influences of SSC, salinity and flow velocity (bottom shear stress) on the formation of kaolinite bedload floccules and consequent bed accretion. This examination of kaolinite behaviour will be followed in the near future (work in progress) by studies of smectite and illite-rich systems that follow the same protocol.

Because the removal of suspended matter from moving suspensions requires particles to settle through a turbulent medium, time is an essential control on how much material arrives at the bottom within a given time span. Letting an experiment run for periods of several weeks will ensure sediment accumulation even at flow velocities that are just slightly below the critical velocity of sedimentation (Schieber *et al.*, 2007), whereas experiments that run for some hours or a few days will require smaller flow velocities to build up a deposit (Schieber, 2011). The latter, however, are flows of interest to the sedimentologist because they compare in duration to flows associated with tidal cycles, river floods and storms, the essential mechanisms that transport mud to depocentres (Schieber, 2016).

Velocity step-down experiments of week-long duration ('Long Drop', *ca* 100 h) were conducted to see clearly the trends in sediment removal from the flow at given velocities. These experiments were then followed by shorter ('Short Drop', *ca* 8 h) experiments that explored a wide range of suspended sediment concentrations. In addition, all experiments were conducted at three salinities: (i) tap water (*ca* 0.00005% mg/l dissolved solids); (ii) 2.0% salinity; and (iii) 3.5% salinity; so as to be able to compare sedimentation characteristics of freshwater, brackish and fully marine settings. Velocity was decreased in 5 cm/s steps for all experiments (Schieber *et al.*, 2007; Schieber, 2011), and the observations collectively suggest that the CVS is located at approximately 25 cm/s. To further

refine that determination an additional set of experiments was added, where the 30 to 20 cm/s velocity range was segmented into five 2 cm/s down-steps. Description of each experiment type is followed by a brief summary of first order interpretations.

Static versus dynamic kaolinite deposition

Although this study is focused on the controls on kaolinite deposition from moving suspensions, evaluating the behaviour in a dynamic setting benefits from knowing how the experimental materials behave under static conditions (gravity settling from still suspensions). It is also important to do this for better comparison of the current results with future studies by other investigators, mainly because not all kaolinites are created equal. For example, even though one might think that a bag of Georgia kaolinite should contain kaolinite with closely similar properties, regardless from where in Georgia it was mined, there can be substantial differences between clays produced from different mines and stratigraphic intervals. For this study, static settling characterization gives guidance with regard to their potential behaviour in flume experiments vis-à-vis SSC and salinity (Fig. 3). Whereas the received wisdom is that kaolinite flocculates and settles more effectively in distilled and freshwater (Parham, 1966; Giese & van Oss, 2002) than in saline waters, Fig. 3 illustrates a more nuanced behaviour for the kaolinite used in this study. At SSCs of 1 g/l or less (typical for rivers; Ellison *et al.*, 2013), kaolinite shows a tendency to settle more effectively in saline waters (Fig. 3), whereas at 10 g/l or higher, freshwater settling outpaces settling in saline waters. The latter is what is commonly reported in the clay mineral literature (Giese & van Oss, 2002), because in practical applications, such as ceramics manufacture, concentrated slurries are the object of interest. At SSCs above 10 g/l, the system enters the realm of liquid muds, commonly encountered in estuaries (Ross & Mehta, 1989; Kineke *et al.*, 1996). Figure 3 does suggest that kaolinite should preferentially get deposited in such settings, validating empirical observations by Parham (1966). Yet, depending on chemical and heat treatments, commercially available kaolinites may deviate significantly from these expectations.

When this same kaolinite is subjected to increasing salinity in a flume running above the

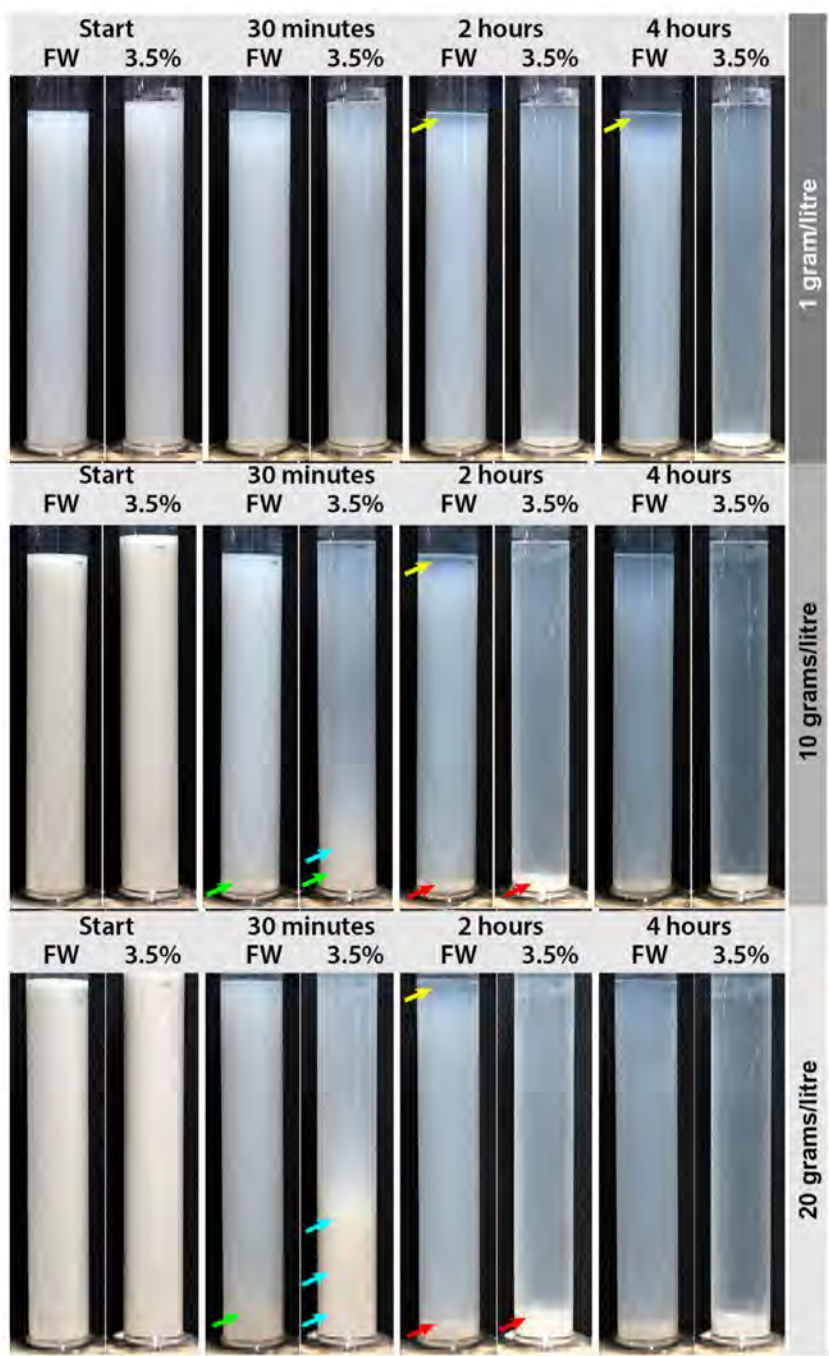


Fig. 3. Settling tube tests of the flume kaolinite in freshwater (FW) and water with 3.5% salinity (2% salinity tests were very similar and are omitted here). Top Row: the 1 g/l experiments (approximately the high end of suspended sediment concentration (SSC) in the flume experiments) show that initially salinity does not make an obvious difference, but by the 2 h mark and forward, the freshwater columns show only a minor clear supernatant (yellow arrows), whereas the saline columns have been cleared of sediment more effectively. Middle Row: the 10 g/l experiments show a distinct change. At the 30 min mark there is a clear fluid–sediment separation for freshwater (green arrows), whereas in the saline column there still is a zone of higher SSC above the fluid–sediment interface (blue arrows). The sediment column in the saline case is thicker than the freshwater case (formed faster and has already compacted more), but by the 2 h mark the settled sediment thickness is the same (red arrows). Bottom Row: the 20 g/l experiments show this contrasting early settling behaviour even more strongly. At the 30 min mark, there is a well-defined fluid–sediment interface for the freshwater case (green arrow), whereas the saline experiment does not yet show a fluid–sediment interface, just a thick zone of high SSC fluid (blue arrows). And whereas at the 2 h mark the ‘saline’ deposit is still thicker than the earlier formed freshwater deposit (red arrows), 2 h later the thickness of the freshwater and ‘saline’ deposits is close to equal, and at 6 h they are the same.

critical velocity of sedimentation, there is essentially a ‘flat’ response from the turbidity sensor. In other words, the measured SSC remains constant as salinity is gradually increased.

First order interpretation

As long as no sediment escapes the flow via bedload formation and sediment deposition (Schieber *et al.*, 2007), salinity has no influence.

In-flow floccule sizes

In initial experiments, observation of flocs was focused on those that travelled over the flume bottom as bedload, because they were comparatively easy to observe and record. When at a later stage the Virginia Tech floc camera system became available, size data of in-flow flocs were added to the already existing data set of repeat experiments. Recording in-flow

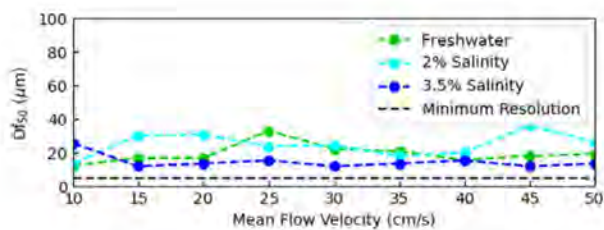


Fig. 4. The size of in-flow particles (presumed to be floccules) in relationship to salinity and flow velocity. In-flow floccules in 2% salinity flows appear overall a bit larger than those seen in freshwater and 3.5% salinity runs, but in general it is observed that in-flow floccules are at best a few tens of microns in size, much smaller than the observed bedload floccules. Initial SSC nominally 231 mg/l for all salinities. For a 30 μm median the lognormal standard deviation is 18.75 to 48 μm, and for all conditions this deviation amounts to $\pm 15 \mu\text{m}$.

floccules from the start of each experiment showed an abundance of in-flow floccules even at high flow velocities and prompted the decision to measure floccule sizes for each velocity step (Fig. 4). Although the floccule data are a bit ‘noisy’ (Fig. 4), it needs to be kept in mind that automated floccule measurement is still a technique under development, and that the data nonetheless show some useful information about in-flow floccule sizes.

Regardless of salinity, in-flow floccules fall into the 10 to 40 μm size range (Fig. 4). Even though the in-flow turbulence gradually decreases as flow velocity is reduced, floccule size appears largely unaffected by this decrease.

First order interpretation

Across the explored velocity range (10 to 50 cm/s; negligible in-flow floccules at 5 cm/s) turbulent shear is sufficient to limit in-flow floccules to a maximum size of approximately 40 μm.

‘Long drop’ experiments

In ‘Long Drop’ experiments 150 g of kaolinite was added to 650 l of water and flow velocities were gradually reduced over a 100 h time interval. Although the sediment addition computes to a nominal suspended sediment concentration (SSC) of 230 mg/l, because the coarse silt portion (Fig. 2A) is largely in bedload at 50 cm/s, the actual initial SSC values fell within the 210 to 230 mg/l range (Fig. 5).

A pertinent observation that can be made in Fig. 5 is that between 50 and 30 cm/s (interval

A in Fig. 5) the velocity reduction steps result in slight drops of SSC, and that the overall SSC decline seems to follow a linear trend (the dashed blue and green lines in Fig. 5). Given that these flow velocities are above what is the likely CVS (Schieber *et al.*, 2007), the decline of SSC probably has two components. The main component is systemic sediment loss in the flume itself. Even if the flume is run at a steady velocity within this velocity range, a long-term (days to weeks) decline of SSC is observed because sediment starts to accumulate (get lost) in the areas before and after the drive belt (Fig. 1A), presumably owing to the increase in effective flow depth (from 5 cm to *ca* 14 cm) and consequent reduction of bottom shear stress. Additional sediment is lost due to secondary flows that deposit sediment on the inside of the turning section sub-channels. The second component, small SSC down-steps that coincide with velocity steps (interval A in Fig. 5), probably are associated with silt particles that transfer from suspension to bedload as flow turbulence decreases. The SSC trendline (dashed green line in Fig. 5) for the freshwater experiment is steeper than that of the saline experiments and signifies a comparatively larger degree of sediment loss. This difference is attributed to the density (buoyancy) difference between freshwater and saline fluids.

For velocities below 30 cm/s, the decline curves for all three salinities depart distinctly (intervals B and C in Fig. 5) from the sediment loss curves that one might attribute to mere sediment loss in the flume (dashed lines in Fig. 5), and the divergence becomes more pronounced as velocity is stepped down further. In all three cases a significant drop of SSC is noted as the velocity is reduced to 25 cm/s (interval B in Fig. 5), with the total drop largest for saline flows. Eleven hours after the 25 cm/s velocity drop SSC values have not stabilized and are still dropping (interval B in Fig. 5), suggesting that the flow velocity is now somewhat below the CVS (Schieber *et al.*, 2007). Reducing the velocity further to 20 cm/s (interval C in Fig. 5) leads to the largest SSC down-steps, with those for saline flows significantly larger than that for freshwater. Reducing velocity further has not much of an impact on SSC decline for freshwater flows. For saline flows, however, stepping down to 15 cm/s leads to further acceleration of sediment loss (Fig. 5). From 15 to 5 cm/s the velocity steps no longer register in the SSC decline curves and indicate continuous transfer

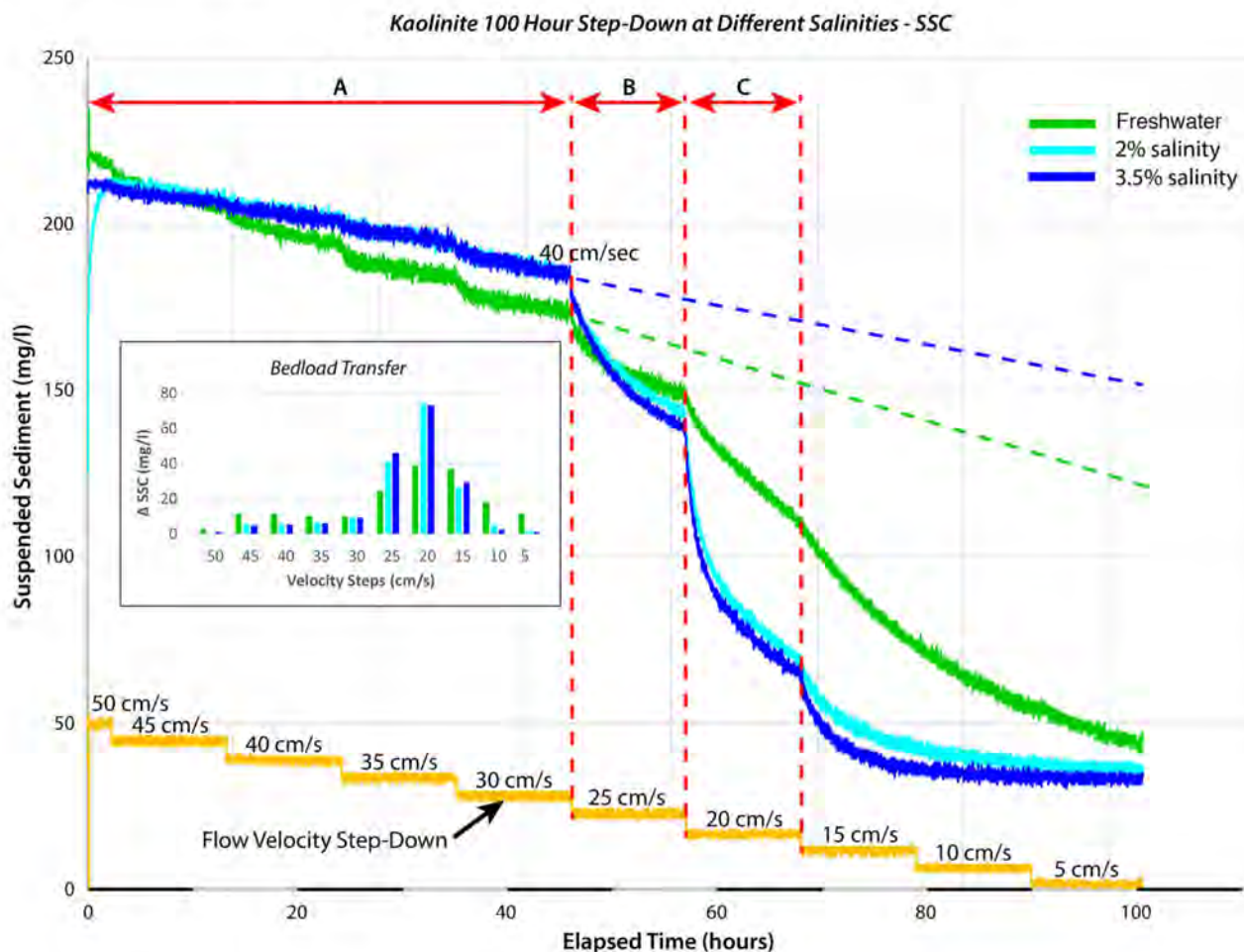


Fig. 5. Suspended sediment concentration (SSC) during step-wise reduction of flow velocity (5 cm/s steps) in variable salinity experiments of 100 h duration. Because all experiments had the same initial sediment loading (150 g), the SSC decline curves are joined at the onset (*ca* 50 cm/s) and then diverge as the velocity is stepped down. Inset shows sediment loss from the flow as velocity decreases.

of sediment to bedload. The bedload transfer inset in Fig. 5 shows that the bulk of bedload is generated in the 25 to 15 cm/s velocity window for all salinities. Yet, whereas saline flows have ‘delivered’ slightly more than 80% of their sediment load by the time the 10 cm/s velocity drop is reached, freshwater flows are about 20% shy of that target at that point and have to continue for at least another 30 h to reach it.

First order interpretation

Figure 5 suggests that, regardless of salinity, the CVS should be below 30 cm/s and somewhat above 25 cm/s, and that increased salinity primarily acts as an accelerant for floccule generation and their transfer to bedload.

‘Short drop’ experiments

In ‘Short Drop’ experiments (8.5 h duration) sediment loading of the flume was increased in five discrete steps (50 g, 100 g, 150 g, 300 g and 600 g; five separate experiments) to explore the influence of SSC (nominally 77 mg/l, 154 mg/l, 231 mg/l, 462 mg/l and 923 mg/l) on the critical velocity of sedimentation. The experiments were conducted in freshwater (five experimental runs), as well as at 2.0% (five experimental runs) and 3.5% salinity (five experimental runs). In this set of 15 experiments bedload floccule sizes were measured for 77 mg/l, 154 mg/l and 231 mg/l in freshwater, and for 231 mg/l in 2.0% and 3.5% saline water (at higher SSC levels floccule photography became difficult). Figures 6 to 8 show the

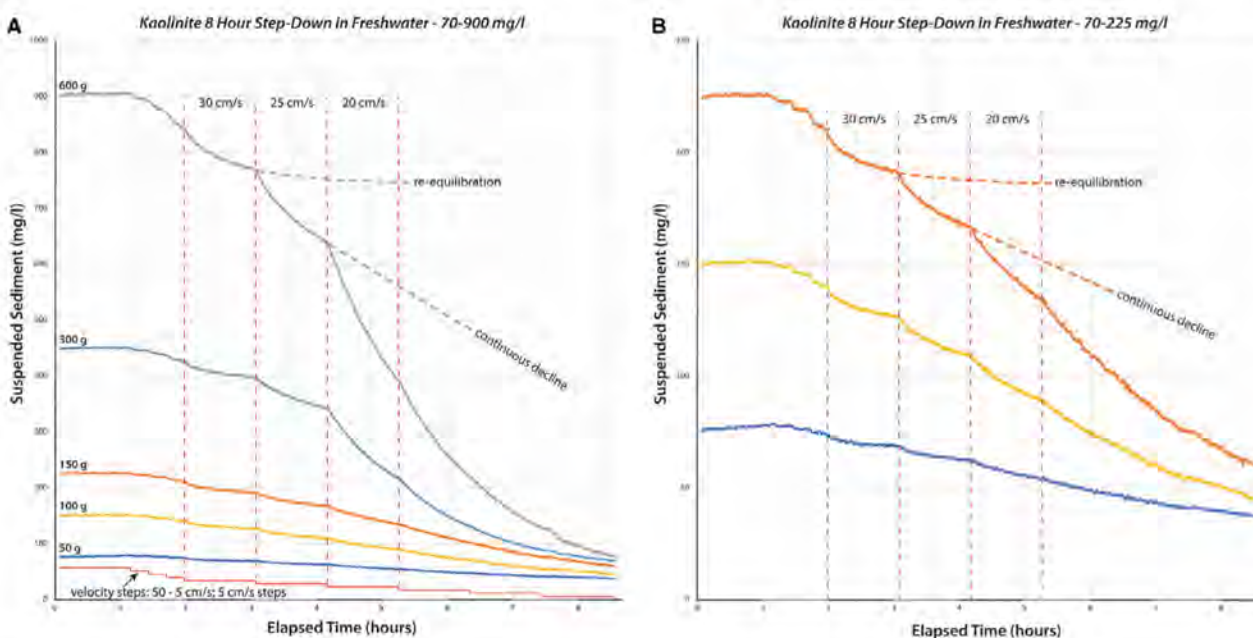


Fig. 6. (A) Suspended sediment decrease with step-wise flow velocity reduction for a wide range of kaolinite loadings in freshwater (50 to 600 g per 650 l of water). (B) Whereas the decline curves for low sediment additions look almost linear in (A), if expanded vertically they show the same characteristics as observed for higher sediment additions in (A).

SSC decline curves for the freshwater, 2.0% salinity and 3.5% salinity ‘Short Drop’ experiments respectively.

Because the ‘Long Drop’ experiments indicate that the critical velocity of sedimentation likely is below 30 cm/s, the freshwater ‘Short Drop’ flume runs (Fig. 6) started at 50 cm/s for about 66 min to ensure optimum suspension of the sediment, and then the 45 cm/s, 40 cm/s and 35 cm/s steps were compressed into 49 min. From 30 to 5 cm/s all steps were again of 66 min duration. Compressing the high velocity ‘Short Drops’ into this time frame was necessitated by the storage capacity of the HD camera used to record bedload floccule development. Dropping velocity by 5 cm/s from 35 to 30 cm/s leads to a freshwater SSC drop that exceeds the SSC drop due to speed reduction from 50 to 35 cm/s (a three times larger velocity reduction), but the decline curve flattens and trends towards re-equilibration (Fig. 6). In contrast the next drop to 25 cm/s results in a sloping decline curve and continuous loss of sediment from the flow, suggesting that the flume now operates below the critical velocity of sedimentation (Schieber *et al.*, 2007; Schieber, 2011). Like in

the ‘Long Drop’ experiments (Fig. 5), the velocity drop from 25 to 20 cm produced the largest sediment transfer to bedload, and the decline curves largely continued at similar slope into the 15 to 5 cm/s velocity region.

Decline curves for the 2.0% and 3.5% salinity ‘Short Drops’ (Figs 7 and 8) are qualitatively no different from the freshwater version of this experiment (Fig. 6). As in the freshwater experiment, the change from re-equilibration to continuous decline occurs at the 25 cm/s step. The main difference between freshwater and saline experiments is (as in the ‘Long Drops’) the steeper decline of SSC from step to step when compared with the freshwater experiment.

First order interpretation

The ‘Short Drops’ show that the critical velocity of sedimentation appears to be the same for SSCs ranging from tens of mg/l to almost a gram per litre. They further confirm and are consistent with the conclusion reached in the ‘Long Drop’ experiments, namely that the CVS is not measurably affected by salinity, and that salt addition largely acts as an accelerant for floc formation.

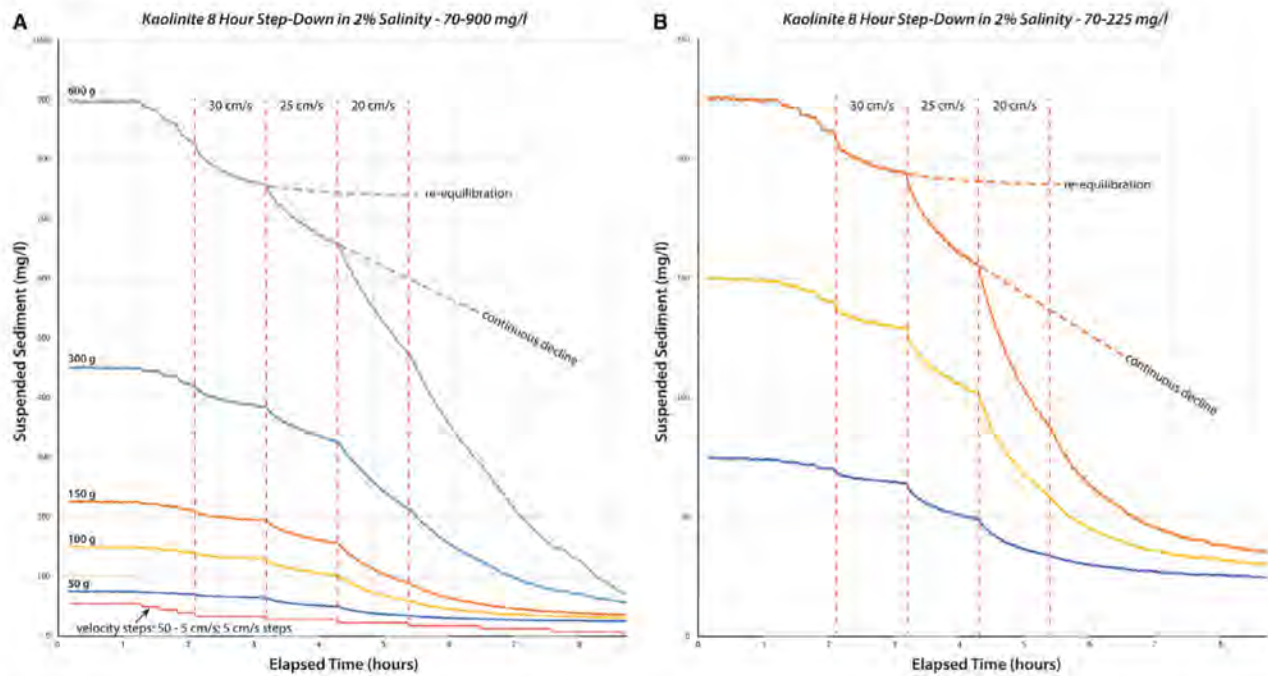


Fig. 7. (A) Suspended sediment decrease with step-wise flow velocity reduction for a wide range of kaolinite loadings in water with 2% salinity. The decline curves for all sediment additions show comparable characteristics. (B) The decline curves for low sediment additions in vertically expanded view. In both (A) and (B), dropping velocity to 30 cm/s leads to initial sediment loss and then re-equilibration with most sediment remaining suspended. As velocity is dropped to 25 cm/s the decline curve steepens for all initial sediment concentrations and suggests continuous decline.

Bracketing the critical velocity of sedimentation

Prior experiments rather firmly bracket the critical velocity of sedimentation for kaolinite as below 30 cm/s and above 20 cm/s, at a provisional 25 cm/s (Figs 5 to 8). In an attempt to better define the CVS in the experimental programme described here, the 30 to 20 cm/s velocity window was examined in detail. Three 150 g experiments were run at freshwater, 2.0% and 3.5% salinity with 2 cm/s velocity steps in the 30 to 20 cm/s velocity range, and the results are shown in Fig. 9.

Whereas Fig. 9 does not provide a precise solution in this quest for a meaningful critical velocity of sedimentation, careful evaluation of the decline curves does allow narrowing down the likely value. Figure 9 shows a distinct difference between freshwater and saline decline curves for the velocity target interval, with freshwater SSCs plotting consistently below the saline SSCs and having less well defined down-steps. This difference reflects the density contrast between freshwater and salt water because floccules experience

improved buoyancy in saline waters. Comparing to Fig. 5 suggests that this buoyancy effect ‘dissipates’ for longer velocity steps (11 h) that allow more time for saline flocs to ‘exit’ the flow. With regard to the critical velocity of sedimentation, the saline SSC decline curves appear to have diagnostic qualities (Fig. 9). The saline decline curves show the same general slope until the velocity reduction to 26 cm/s, and then cross-over at the 24 cm/s velocity reduction. The SSC drop increases somewhat between the 30 to 28 cm/s velocity reduction (A) and the 28 to 26 cm/s velocity reduction (A + B), suggesting that the critical velocity is below 28 cm/s. A significant increase of SSC drop (A + B + C) is observed at the next velocity reduction step (26 to 24 cm/s), suggesting that a threshold had definitely been crossed. An even steeper SSC drop for the 24 to 22 cm/s velocity interval suggests that the critical velocity is definitely above 24 cm/s.

First order interpretation

Based on the above observations one can reason that the critical velocity is likely slightly above



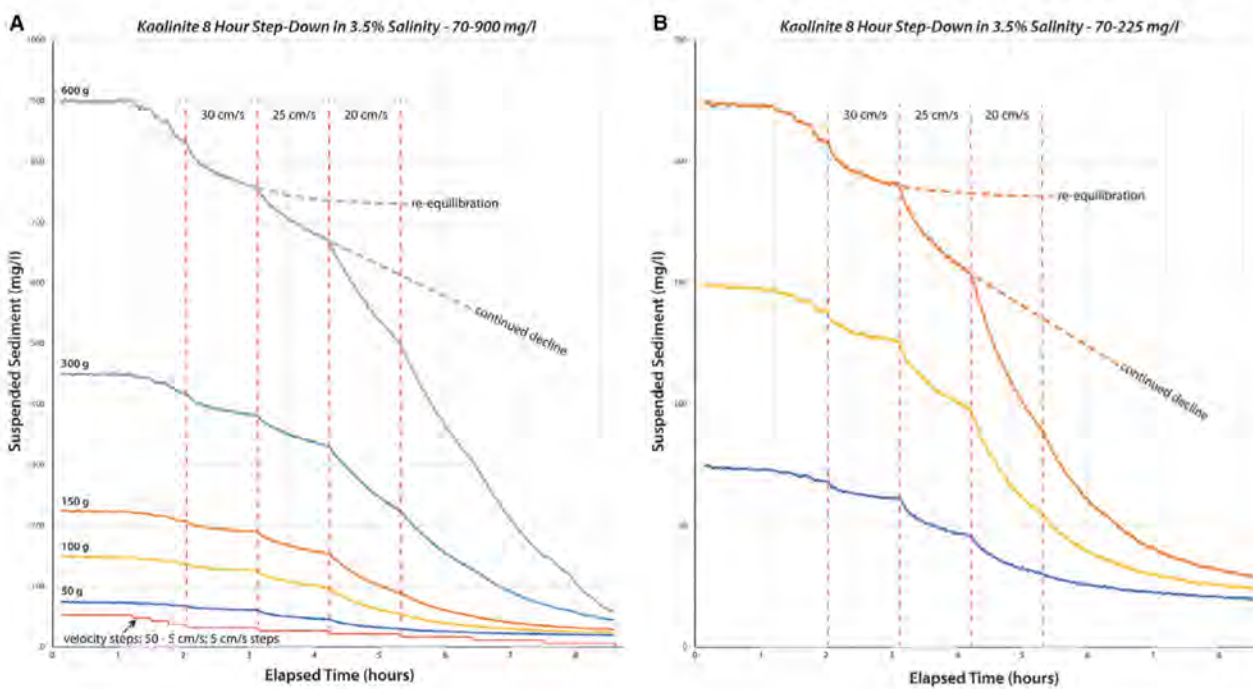


Fig. 8. (A) Suspended sediment decrease with step-wise flow velocity reduction for a wide range of kaolinite loadings in water with 3.5% salinity. The decline curves for all sediment additions show comparable characteristics. (B) The decline curves for low sediment additions in vertically expanded view. In both (A) and (B), dropping velocity to 30 cm/s leads to initial sediment loss and then re-equilibration with most sediment remaining suspended. As velocity is dropped to 25 cm/s the decline curve steepens for all initial sediment concentrations and suggests continuous decline.

26 cm/s and below 28 cm/s. Given that the flow meters in use are at best accurate within ± 1 cm/s and are subject to temperature drift along with the control electronics for the flume motor, all that can realistically be said is that the critical velocity at room temperature (*ca* 20°C) is likely located between 26 and 28 cm/s. Unpublished threshold of motion tests for sand grains in the flumes at the IU Shale Research Lab indicate a value of 22 cm/s for medium to coarse sand. Thus sand grains can move in bedload at the same time as kaolinite bedload flocs (Schieber *et al.*, 2007; Yawar & Schieber, 2019).

Bed formation and the size of bedload flocs

In addition to velocity and SSC data, the above-described experiments were accompanied by recording sediment accumulation in the form of ripples and bed accretion for each experiment. These observations parallel the inferences made from SSC data and show the onset of silt and floccule ripples, as well as growing bed coverage

in the course of experiments. The information about the onset of bedload floccule formation is consistent for all of the time-lapse image sets but becomes clearer as sediment loading increases and enough floccules are available to form multiple ripples and cover the flume bed (Fig. 10).

The image insets from Fig. 10 illustrate the physical processes that correlate to the SSC decline curves discussed in preceding figures. At 40 cm/s (inset a) only boundary layer streaks are visible. At 35 cm/s (inset b) denser, fast migrating portions of boundary layer streaks become visible (yellow arrow). These are considered incipient coarse silt ripples (Yawar & Schieber, 2017) that represent the approximately 5 wt.% of the kaolinite feed that exists as solid kaolinite particles larger than 0.02 mm (Fig. 2A). At 30 cm/s (inset c) well-developed ripples appear, and some of them are developing trailing 'tails' (yellow arrow) that seem to adhere to the flume bottom. Once velocity has dropped below the CVS as inferred from SSC data (see above), many of the ripples now leave behind

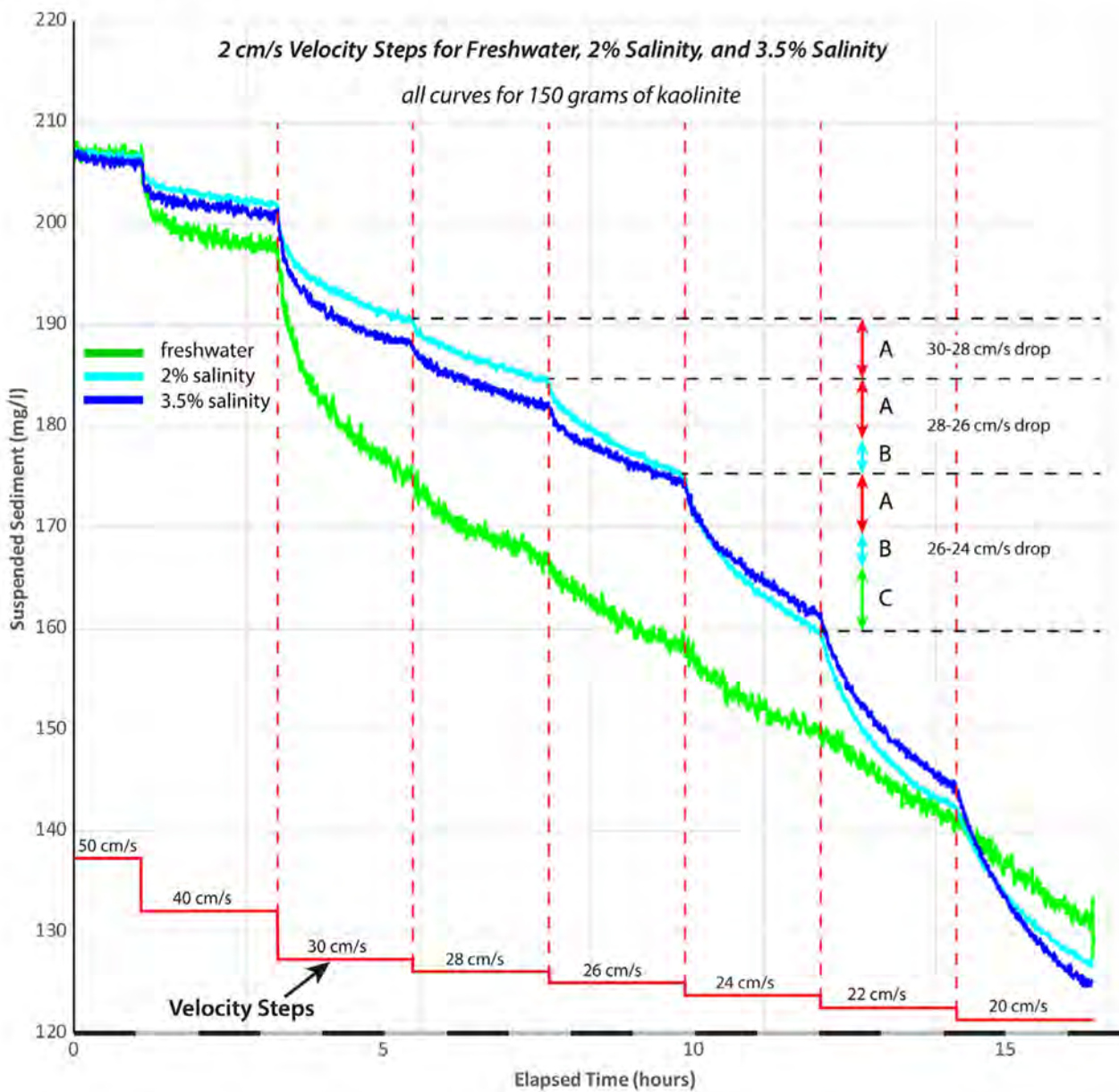


Fig. 9. Targeting the critical velocity of sedimentation with 2 cm/s velocity steps. For the 30 to 28 cm/s velocity reduction the suspended sediment concentration (SSC) drop (A) for saline flows is similar in slope to the previous velocity step. For the 28 to 26 cm/s velocity reduction, the SSC drop increases fractionally (B) relative to the previous velocity step. For the 26 to 24 cm/s velocity reduction, the SSC drop increased significantly in magnitude (C), suggesting that a threshold had definitely been crossed.

adhering ‘tails’ (inset d). At 20 cm/s (inset e) ‘tail’ formation extends further and the flume bottom increasingly is covered with adhering ripple ‘tails’. This trend of increasing bed coverage continues at 15 cm/s (inset f), and by the time 10 cm/s is reached most of the suspended sediment has been deposited (inset g) and, depending on total sediment available, the flume

bottom will be covered with ripple deposited flocculated kaolinite.

The correspondence between information gleaned from flow monitoring and observations of bedload sediment illustrated in Fig. 10 extends further to the size of bedload floccules as recorded by HD cameras in macro-mode (Fig. 11). Floccule images from across the

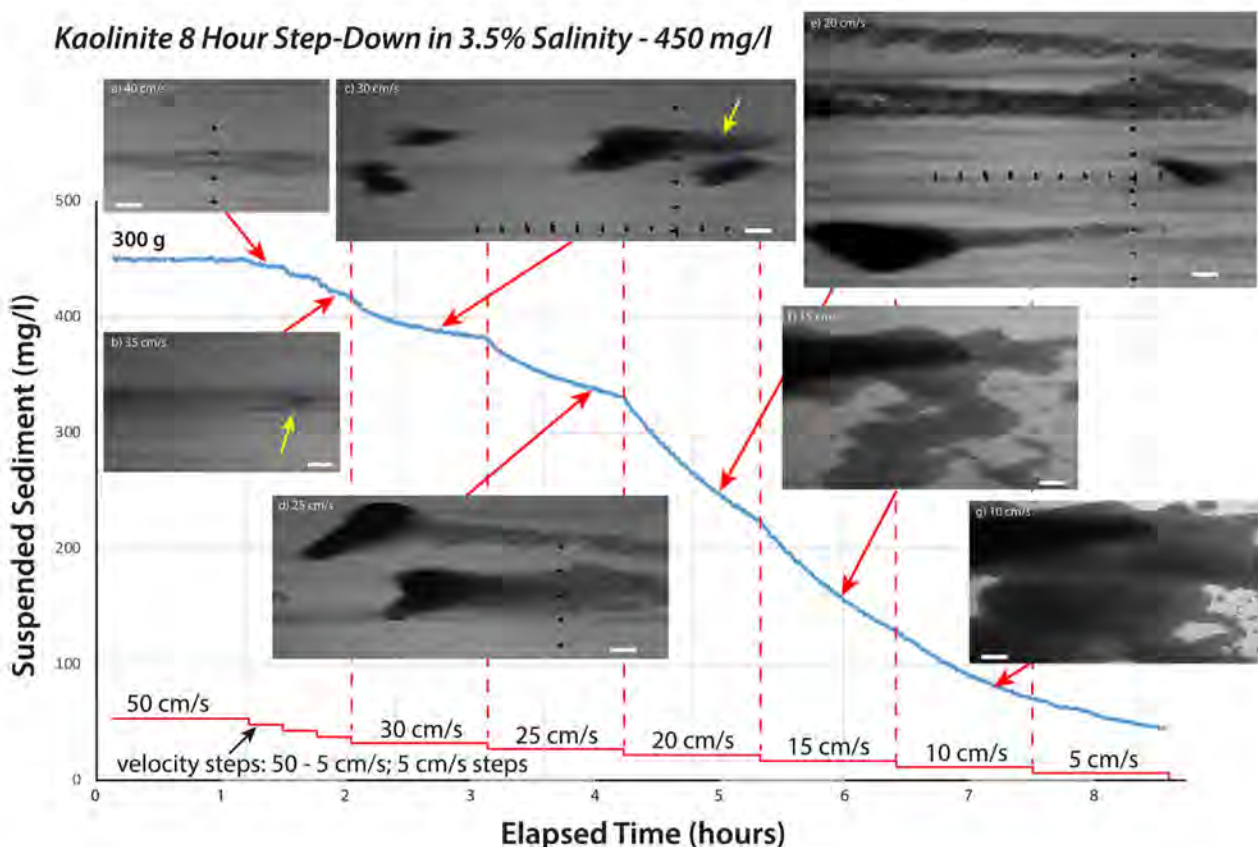


Fig. 10. Visual manifestations of floccule accumulation at the flume bottom in relation to velocity steps, from an experiment where the initial suspended sediment concentration was 450 mg/l and the water had 3.5% salinity. Where in time (x-axis) the flume bottom image insets (labelled a to g) come from is marked with red arrows that connect the images to the decline curve. The yellow arrow in inset b points to denser, fast migrating portions of boundary layer streaks. The yellow arrow in inset c points to a trailing 'tail' that seems to adhere to the flume bottom.

velocity steps of above experiments consistently show that at velocities above 25 cm/s the only discernible particles are silt size, and that once 25 cm/s is reached sand size particles are visibly present (Fig. 11).

First order interpretation

The sand-size particles observed at velocities of 25 cm/s and lower are presumed to be clay flocs, by virtue of the fine-grained nature of the sediment feed (Fig. 2) that is devoid of sand size particles. There is also a general trend of particle size increase (to the left) as bed shear τ drops further below 0.2 Pa. The visible onset of sand-size bedload flocs occurs at the same velocity step (30 to 25 cm/s) irrespective of sediment loading and salinity.

The HD video clips used to illustrate floccule size in Fig. 11 were also evaluated statistically

for particle size (Fig. 12). Film clips were subsampled for frames (450 mm^2) with good contrast and focus, and for each velocity particle sizes were measured manually with ImageJ for seven to ten frames. The results are shown as violin plots in Fig. 12 which quantitatively presents the size distributions of flocs under different shear stress conditions, an aspect that cannot be derived directly from photographs of flocs at the flume base (Fig. 11). The violin plots used to compile Fig. 12 are a more accurate way to illustrate floccule size distributions than single average values of floccule size or box plots and show that overall flocs increase in size with decreasing shear stress, regardless of the experimental conditions.

The violin plots in Fig. 12 reflect normalized probability densities of the data that were scaled to the same width. This method of data

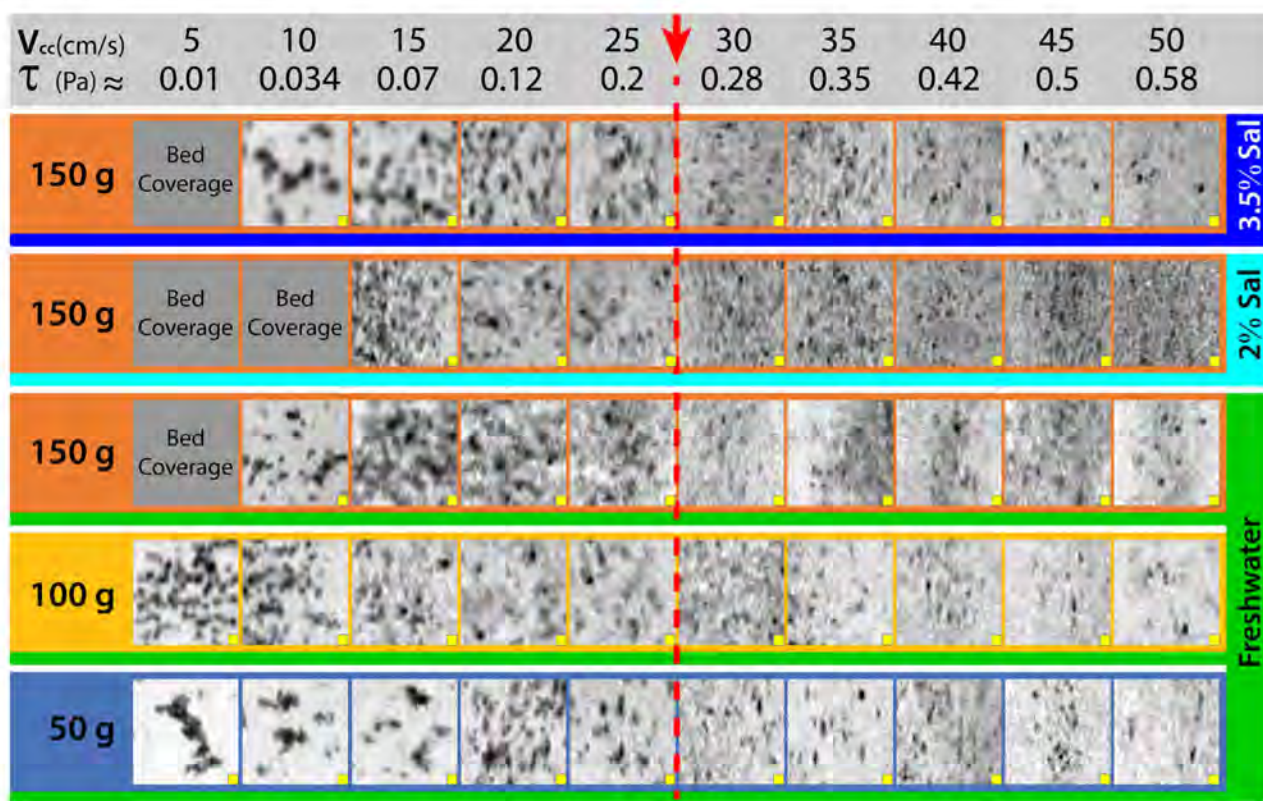
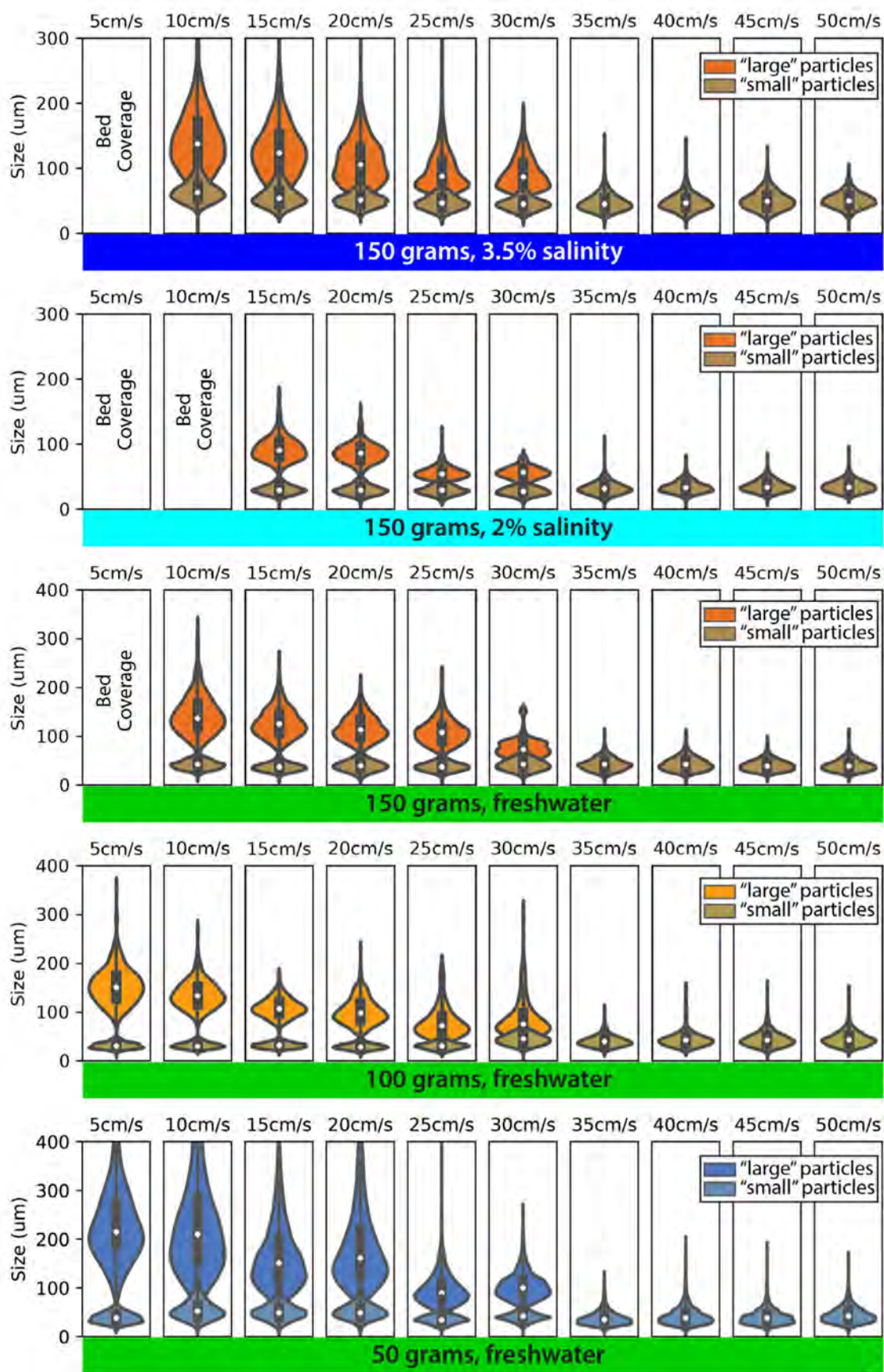


Fig. 11. High definition (HD) video camera sub frames (1 mm by 1 mm) that show particles travelling over the flume bottom at various sediment loadings, flow velocities, bed shear and salinities. Yellow squares are 100 µm wide. Vertical elongate particles in the right half of the figure are caused by motion blur at higher flow velocities. Red arrow and dashed red line separate flow velocities above (to the right) and below (to the left) the critical velocity of sedimentation.

presentation was used because the raw data sets collected from film frames required ‘judgement calls’ on where in a given frame to measure particles (avoiding out of focus regions, as well as overcrowded portions). Thus from experiment to experiment the base data lacked uniformity, and simply comparing averages would have been statistically unsound. Despite these shortcomings, every effort was made to fully characterize the floccule size distribution by measuring as

many floccules as possible. Because of the required ‘judgmental calls’ and differences in floccule density from frame to frame under different shear stress conditions, the total number of measured floccules does not reflect the abundance of floccules under a given experimental condition – more frames/areas were measured if floccule density was low and fewer frames/areas were measured if floccule density was high. However, this approach is able to generally

Fig. 12. Violin plots that show the distribution of particle sizes measured at the flume bed under variable experimental conditions. The box plot inside each violin plot shows the median (the white dot) and inter-quartile range (the black box) of the particle size. The overall shape of a given violin plot represents the probability density of the data, with wider visual distribution indicating a higher density. The width of each violin was scaled to be the same. ‘Small’ particles = data sets dominated by particles <63 µm; ‘Large’ particles = data sets dominated by particles >63 µm. Particle and floccule sizes were measured from HD camera frames for the same experiments as shown in Fig. 11 and show onset of large floccule formation once velocity is reduced to 30 cm/s, followed by continued floccule formation and gradual increase of floccule size as bed shear (velocity) is reduced further. Bed shear stress values associated with the various flow velocities are shown in Fig. 11.



capture the floccule size distribution because more than 500 floccules (and typically multiples of that number) were measured under every experimental condition. Image frames were processed manually by multiple operators for a large number of film frames and show the same overall trends for all experiments. Collectively, and together with the actual floccule images in Fig. 11, this suggests that potential statistical bias did not obscure the underlying realities of grain-size distribution.

First order interpretation

As presented in Fig. 12, the data show unequivocally that, across the entire extent of these experiments, the derived size trends support the notion (as gleaned from Fig. 11) that there is an increase of floccule size with decreasing shear stress that holds true for all experimental conditions.

Although the scaling of the violin plots (Fig. 12) might at first suggest that sand-size floccules become significant at 30 cm/s, having a direct look at film frames indicated otherwise. For example, comparing film frames for 30 cm/s (Fig. 13A) with those taken at 25 cm/s (Fig. 13B) from the 50 g freshwater data set (Fig. 12), shows that sand size floccules are significantly less abundant at

30 cm/s. That large floccule formation is barely starting at 30 cm/s is also indicated in Fig. 5, where significant bedload transfer starts at flow velocities of 25 cm/s.

The appearance of sand size floccules at 30 cm/s ties in with the formation of elongate ripple 'tails' as seen in Fig. 10 (inset c; 30 cm/s). However, unlike in Fig. 10 inset d (25 cm/s), these (30 cm/s) 'tails' do not have permanence and disappear as the ripple passes. Given that significant bedload transfer of sediment occurs once velocity is reduced to 25 cm/s (Fig. 5), the initial occurrence of sand size floccules at 30 cm/s can therefore be considered as an indication that the system approaches critical velocity, whereas the sharp increase in the abundance of sand-size floccules at 25 cm/s (Fig. 13B) indicates that the flow is now below the critical velocity of sedimentation.

DISCUSSION AND OUTLOOK

The main finding of this study is somewhat counterintuitive: namely that in moving kaolinite suspensions the critical velocity of sedimentation (CVS) is a stable quantity in spite of large variations of suspended sediment concentration

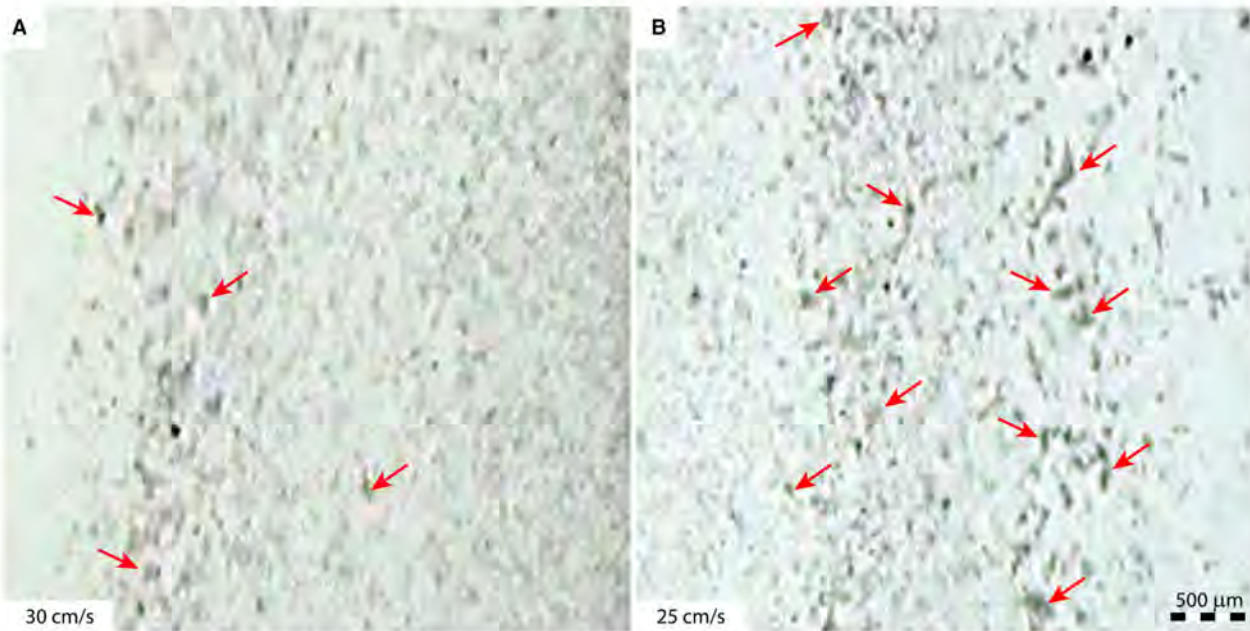


Fig. 13. Comparison of 30 cm/s (A) and 25 cm/s (B) film frames for the 50 g freshwater experiment. Sand size floccules are present at 30 cm/s (representative examples marked with red arrows), but they are much more abundant at 25 cm/s (representative examples marked with red arrows).

(SSC) and salinity. Extending to the real world, where muds contain various other clays instead of kaolinite (Potter *et al.*, 2005; Lazar *et al.*, 2015) as well as a sizeable silt fraction, this could suggest a deceptively simple conceptual framework for mudstone sedimentology: one critical velocity per clay mineral, or better even, a narrow range of critical velocities that works for a wide compositional range of muddy suspensions. The observations presented here agree with previously published observations on the deposition of flocculated clays from moving suspensions (Schieber *et al.*, 2007; Schieber, 2011). Yet, unlike these earlier studies, the set of experiments and associated data presented here constitute a much more systematic and focused exploration of key factors that supposedly govern flocculation and deposition of clays (Kranck, 1973; McCave, 1975; Mehta *et al.*, 1989; Syvitski *et al.*, 1995; Manning & Dyer, 1999; Stone & Krishnappan, 2003; Mietta *et al.*, 2009; Safak *et al.*, 2013). Whether what was learned from these experiments will hold true for other clays and other fine-grained sediments in general remains to be seen, but clearly needs to be explored further.

Kaolinite is no ordinary clay. Studied since at least the 17th century as the raw material for high quality ceramics, much is known about its behaviour in colloidal suspensions. In a recent assessment of the state of the art in clay behaviour, Giese & van Oss (2002) state succinctly that whereas most clays tend to form stable suspensions at low ionic strengths (distilled and freshwater) and are more prone to flocculate at high ionic strength (saline; Verwey & Overbeek, 1948), kaolinite does the exact opposite and can even flocculate in distilled water (Schofield & Samson, 1954). This peculiar behaviour is attributed to the comparatively thick edges of kaolinite particles that cause flocculation in a sturdy house-of-cards arrangement (van Olphen, Van Olphen, 1977). If examined in some detail, there is an immense literature on clay flocculation including kaolinite (Goldberg & Glaubig, 1987; Lagaly, 2006; Zbik *et al.*, 2008) that shows how clay properties, including flocculation, can be engineered for specific applications through additives and other treatments. To become cognizant of the latter quickly disabuses any investigator of the idealistic notion that a given commercially available clay should have unambiguous flocculation properties. So, for the experimentally inclined sedimentologist this then begs the question of where to source

kaolinite that is to be used in experiments that may have relevance for sedimentology. The decision to use Acti-Min SA1 kaolin for these experiments grew out of consultations with the late Dr Haydn Murray, a colleague with extensive expertise in clay minerals and a broad knowledge of the clay industry. The challenge was to find a kaolin that had not been engineered and whose properties were close to kaolinites that are common in young clay-rich strata, like those from the lower Mississippi valley, the Mississippi delta and adjacent shelf regions. Dr Murray recommended Acti-Min SA1 as a suitable proxy, and this clay has therefore been used exclusively in all kaolinite-based experiments at the IU Shale Research Lab. Another challenge for comparing the flocculation observed in the current experiments with what is published in the clay mineral literature is that these earlier studies did not examine flocculation in the context of moving suspensions, but rather from settling in still water (Fig. 3). Whereas we record floccule formation in our experiments, know the parameters associated with floccule formation (flow velocity, SSC, salinity, etc.), and are even able to make pictures of those fortuitously collected (Fig. 2E; Schieber *et al.*, 2007; Schieber, 2011), it is acknowledged that muddy sediments are highly complex systems that may require as many as 32 variables and parameters to be considered for full physicochemical characterization (Berlamont *et al.*, 1993).

The flow in the described experiments is fully turbulent (R_e ca 7119 to 71 190; see Appendix S1) and hydraulically smooth, and a turbulent boundary layer exists between the flow boundary (flume wall) and the turbulent interior of the flow. Three qualitatively different but intergrading zones of flow can be recognized (Fig. 14), a thin viscous sublayer next to the wall, a turbulence-dominated outer layer that occupies most of the flow depth and a buffer layer between them (Middleton & Southard, 1984). With the given flume dimensions (Fig. 1) the viscous sublayer should be on the order of a millimetre or less in thickness and will be the flow region with the highest shear rate (Middleton & Southard, 1984). That basic fact of fluid dynamics is a matter of concern, because high shear is, generally speaking, detrimental to floccules (Milligan & Hill, 1998; Manning & Dyer, 1999; Hill *et al.*, 2001; Haralampides *et al.*, 2003). Figure 12 shows that above the critical velocity of sedimentation, bedload particles fall into the medium to coarse silt size range. As pointed out above (see Bed

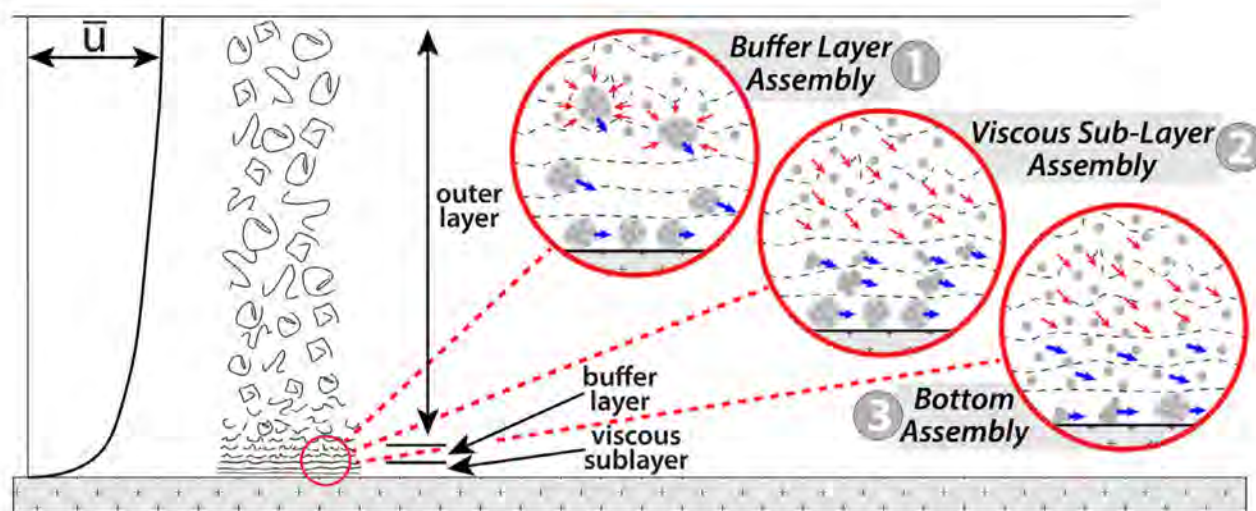


Fig. 14. A definition sketch (not to scale) of a turbulent boundary layer (after Middleton & Southard, 1984) and three possible scenarios (large red circles) for producing sand size bedload floccules. Arrows indicate overall motion of in-flow floccules and larger composite grains. The small grey dots represent in-flow floccules that are merged into larger aggregates.

formation and the size of bedload floccules) these particles probably represent those ca 5% of the clay feed that occupies the medium to coarse silt size range (Fig. 2A), and consist of solid kaolinite particles (clasts). These particles are observed as a distinct grain population that persists in bedload throughout the experiments (Fig. 12). It is plausible to assume that in the velocity range from 35 to 50 cm/s bed shear simply is too strong to allow floccules of any kind to pass to the bed and be stable.

Floccule imaging shows that bedload floccules up to several hundred microns in size (Fig. 12) start to appear at the base of the flow (Fig. 12) once the flow velocity is reduced to 30 cm/s ($\tau = 0.28 \text{ Pa}$, Fig. 11), and form *en masse* once velocity drops to 25 cm/s ($\tau = 0.2 \text{ Pa}$, Fig. 11) and lower (Figs 5 and 12) in spite of the high shear regime at the base of the flow. In the *Introduction* this problem was referred to as the 'basal shear conundrum'. Another observation that bears repeating in this regard is the fact (Fig. 4) that in-flow floccules are at best a few tens of microns in size, regardless of flow velocity and salinity. This observation in essence precludes that large bedflow floccules could have formed in the main body of the flow and then simply settled through the viscous sublayer to the bottom.

Given that the in-flow floccules were imaged at half-height (5 cm) within the flow leaves open the possibility that large floccules formed in the turbulent flow boundary layer (viscous sublayer,

buffer layer or even at the very bottom of the flow), but to image in-flow floccules that close to the bed poses technical challenges. Currently the submerged light source for in-flow floccule imaging is comparatively bulky (ca 30 cm^3 displacement) and prone to completely disrupt the near bed flow if it were deployed close to the bed. Scientific equipment has been miniaturized to an amazing degree for use on spacecraft and landed rovers, giving hope that there is probably a technical solution for this. At the moment, however, it is not within the grasp of researchers. On the other hand, the fully turbulent nature of the flow should ensure that over a matter of seconds the sidewall floc camera 'sees' floccules from across the flow height. If there were large floccules forming 'in-flow' they should be captured. Their apparent absence challenges the observer to think of alternative scenarios.

When it comes to the origin of the sand size floccules that dominate the left side of Figs 11 and 12, one can therefore envision several possible scenarios of origin (Fig. 14). At flow velocities of 30 cm/s larger particles, presumed to be floccules, start to appear in HD image frames (Figs 11 and 13A), and then significantly increase in abundance once the flow slows to 25 cm/s and below (Fig. 13B). At present, the assumption is that small in-flow floccules assembled into larger aggregates near the base of the flow (Fig. 14). As discussed above, from what is currently known about the size of in-

flow floccules, the larger floccules could for example have formed in the buffer layer before transiting through the viscous sub-layer (buffer layer assembly, option 1 in Fig. 14). The observed increase of bedload floccule size with decreasing shear stress (Figs 11 and 12) may mean that as the shear differential in the sub-layer decreased, larger and larger floccules were able to pass the 'shear filter'. Alternatively, in-flow floccules could have entered the viscous sub-layer, and as those floccules moved horizontally at different speeds within successive (imaginary) 'laminae' of the sub-layer they could have collided and step by step been combined into larger aggregates. This is option 2, designated as 'viscous sub-layer assembly', in Fig. 14. Here as well, decreasing shear differential would yield larger floccules as flow velocity decreased. In option 3, 'bottom assembly', in-flow floccules transit through the viscous sub-layer and then form larger aggregates once they have reached the bed (Fig. 14). Option 3 has a less implicit connection to the shear differential, but it can be surmized that larger aggregates have better preservation potential at reduced levels of bottom shear. It is conceivable that all three mechanisms (Fig. 14) are active at certain parts of the velocity spectrum, with option 3 dominant just below the CVS, option 1 towards low velocities and option 2 in the interim. This issue will be addressed in detail in future studies.

Although flume experiments with clays lack the complexity inherent in natural sediment mixtures, experience from multiple experiments with other materials and natural muds (Schieber, 2011) suggest that they do convey perspectives to be cognizant of when interpreting the rock record. With that caveat in mind, it appears for example that assuming critical velocities in the 30 to 20 cm/s window for natural muds is useful guidance for interpreting environmental parameters. Likewise, the rates of sediment loss that can be derived from the SSC decline curves can inform about how much post-compaction thickness to expect approximately from natural flows of a few days duration, and how that thickness might be distributed across the length of the resulting deposits. For example, at comparatively high SSC (*ca* 4 g/l) a net accumulation of 10 mm per week is readily achievable from a flow of 10 cm thickness, and with an assumed initial water content of 85% the rock record equivalent would be 1.5 mm thick. Thus, assuming a turbid flow of a few days duration for a natural deposit

of a given thickness, plausible SSC values (from experiment or field measurements) could be selected and used to estimate the thickness of the originating flow. As such, the experiments provide first order mass balance benchmarks for interpreting perceived rock record equivalents.

CONCLUSIONS

This study represents a systematic flume study of the factors that control the formation of bedload floccules and bed accretion in moving kaolinite suspensions. A key result is that up to suspended sediment concentrations of 0.9 g/l at least, there is no measurable influence of suspended sediment concentration (SSC) on the critical velocity of sedimentation (CVS). In addition, the CVS is insensitive to flow salinity (freshwater, brackish water, fully marine). Salt added to the flow primarily acts as an accelerator; it increases flocculation efficiency. The CVS for the kaolinite used in these experiments is in the 26 to 28 cm/s range, equivalent to a bed shear stress of 0.22 to 0.25 Pa. The suspended floccules in the flow are a few tens of microns in size, and their size seems largely insensitive to salinity. SSC decline curves are very valuable for evaluating the flocculation behaviour of moving suspensions of clays and other fine-grained materials. Derived critical velocities of sedimentation match those gathered from floccule imaging and require significantly less effort to acquire. SSC decline curves also allow quantification of sediment deposition for given flow conditions and durations.

An important take home message from above discussion is that the formation of large bedload floccules represents a bed shear stress effect. Neither suspended sediment concentration nor salinity can 'force' floccule formation, but rather bed shear has to fall below a threshold level before large bedload floccules can assemble at the base of the flow. Once that process has started, sediment is continuously sequestered from the flow and suspended sediment concentration is allowed to drop until very little sediment remains in the flow. Yet, whereas this can be said with considerable confidence for kaolinite, whether other clays or fine-grained sediments show comparable behaviour will require additional experimentation. There is certainly the potential that, just like kaolinite, other flocculation prone sedimentary components have an intrinsic critical velocity of sedimentation that is insensitive to SSC and salinity.

How exactly sand size bedload floccules originate in the presence of high shear rates remains an unresolved issue. Currently three options of large floccule formation (Fig. 14) seem feasible. First: assembly in the buffer layer; second: assembly *via* collision in the viscous sub-layer; or third: bottom of flow assembly from in-flow proto floccules. Future progress in understanding how large floccules form in the base of these flows, flows that have the capacity to move actual sand grains of much higher density (quartz, feldspar, etc.), will hinge on the ability to actually observe floccule motion in the bottom few millimetres of muddy suspensions. A technical solution using a combination of sheet lasers and high speed cameras should be possible, and the challenge is to find a design that minimizes (or eliminates) interference with the flow itself. Yet, even without knowing the exact mechanism that gives rise to sand-size bedload floccules, their existence is irrefutable. We know that the onset of their formation is conditioned on flow velocity/bed shear stress, that there is a rather specific critical velocity (shear stress) of sedimentation, and that flows that move slower than that critical threshold give rise to migrating floccule ripples and clay/mud-bed accretion.

Given that clays can show significant variability of properties even within a given class (for example, kaolinite), restraint is advisable when trying to extend results from this study to other clays or muds and mudstones in general. Comparable experimental studies need to be conducted for other clays, as well as fine-grained sediment mixtures, to constructively apply this type of data to sedimentological studies.

ACKNOWLEDGEMENTS

Funding for this research was provided by the sponsors of the IU Shale Research Consortium (Anadarko, Chevron, ConocoPhillips, ExxonMobil, Shell, Statoil, Marathon, Whiting, and Wintershall). A National Science Foundation equipment grant to J. Schieber (EAR-0318769) provided funds for the purchase of the analytical SEM that was used to acquire SEM images for this article. The paper also benefited from constructive suggestions by Drs João Trabuchó-Alexandre, Aubry DeReuil, Lauren Birgenheier, Peir Pufahl, Chris Paola and an anonymous reviewer. Dr David Bish of the Indiana University Department of Chemistry kindly provided the quantitative analysis of the kaolinite clay

used in these experiments, as well as his insights into the peculiarities of industrially sourced kaolinite. We also thank Dr Juan Fedele from the ExxonMobil Research Labs for computing bed shear stress values from provided velocity profiles.

DATA AVAILABILITY STATEMENT

Data utilized for preparation of this paper are archived at the IU Shale Research Lab and are available upon reasonable request.

REFERENCES

- Aplin, A.C. and Macquaker, J.H.S. (2011) Mudstone diversity: origin and implications for source, seal, and reservoir properties in petroleum systems. *AAPG Bull.*, **95**, 2013–2059.
- Asmala, E., Bowers, D.G., Autio, R., Kaartokallio, H. and Thomas, D.N. (2014) Qualitative changes of riverine dissolved organic matter at low salinities due to flocculation. *J. Geophys. Res. Biogeo.*, **119**, 1919–1933.
- Baas, J.H. and Best, J.L. (2002) Turbulence modulation in clay-rich sediment-laden flows and some implications for sediment deposition. *J. Sed. Res.*, **72**, 336–340.
- Berlamont, J., Ockenden, M., Toorman, E. and Winterwerp, J. (1993) The characterization of cohesive sediment properties. *Coast. Eng.*, **21**, 105–128.
- Burban, P.-Y., Lick, W. and Lick, J. (1989) The flocculation of fine-grained sediments in estuarine waters. *J. Geophys. Res. Oceans*, **94**, 8323–8330.
- Burt, T.N. (1986) Field settling velocities of estuary muds. In: *Estuarine Cohesive Sediment Dynamics* (Ed Mehta, A.J.), pp. 126–150. Springer, New York, NY.
- Chang, T.S. and Flemming, B. (2013) Ripples in intertidal mud—a conceptual explanation. *Geo-Mar. Lett.*, **33**, 449–461.
- Clauser, F.H. (1954) Turbulent boundary layers in adverse pressure gradients. *J. Aeronaut. Sci.*, **21**, 91–108.
- Einstein, H. and Li, H. (1956) The viscous sublayer along a smooth boundary. *J. Eng. Mech. ASCE*, **82**, 1–7.
- Ellison, C.A., Savage, B.E. and Johnson, G.D. (2013) Suspended-sediment concentrations, loads, total suspended solids, turbidity, and particle-size fractions for selected rivers in Minnesota, 2007 through 2011. *USGS Sci. Inv. Rep.*, **2013-5205**, 56.
- Furukawa, Y., Reed, A.H. and Zhang, G. (2014) Effect of organic matter on estuarine flocculation: a laboratory study using montmorillonite, humic acid, xantham gum, guar gum and natural estuarine flocs. *Geochem Trans.*, **15**, 1.
- Ghadeer, S.G. and Macquaker, J.H.S. (2011) Sediment transport processes in an ancient mud-dominated succession: a comparison of processes operating in marine offshore settings and anoxic Basinal environments. *J. Geol. Soc. London.*, **168**, 1121–1132.
- Giese, R.F. and van Oss, C.J. (2002) *Colloid and Surface Properties of Clays and Related Minerals*, p. 312. CRC Press, New York, NY.
- Goldberg, S. and Glaubig, R.A. (1987) Effect of saturating cation, pH, and aluminum and iron oxide on the

- flocculation of kaolinite and montmorillonite. *Clays Clay Miner.*, **35**, 220–227.
- Haralampides, K., McCorquodale, J.A. and Krishnappan, B.G.** (2003) Deposition properties of fine sediment. *J. Hydraul. Eng.*, **129**, 230–234.
- Hill, P.S., Voulgaris, G. and Trowbridge, J.H.** (2001) Controls on floc size in a continental shelf bottom boundary layer. *J. Geophys. Res. Oceans*, **106**, 9543–9549.
- Keyvani, A. and Strom, K.** (2013) A fully-automated image processing technique to improve measurement of suspended particles and flocs by removing out-of-focus objects. *Comput. Geosci.*, **52**, 189–198.
- Kineke, G.C., Sternberg, R.W., Trowbridge, J.H. and Geyer, W.R.** (1996) Fluid mud processes on the Amazon continental shelf. *Cont. Shelf Res.*, **16**, 667–696.
- Kranck, K.** (1973) Flocculation of suspended sediment in the sea. *Nature*, **246**, 348–350.
- Lagaly, G.** (2006) Colloid clay science. In: *Handbook of Clay Science* (Eds Bergaya, F., Theng, B.K.G. and Lagaly, G.), pp. 141–245. Elsevier, Amsterdam.
- Lamb, M.P., de Leeuw, J., Fischer, W.W., Moodie, A.J., Venditti, J.G., Nittrouer, J.A., Haught, D. and Parker, G.** (2020) Mud in rivers transported as flocculated and suspended bed material. *Nat. Geosci.*, **13**, 1–5.
- Lazar, R., Bohacs, K.M., Schieber, J., Macquaker, J. and Demko, T.** (2015) Mudstone primer: lithofacies variations, diagnostic criteria, and sedimentologic stratigraphic implications at the lamina to bedset scale. *SEPM Con. Sed. Paleo.*, **12**, 198.
- van Leussen, W.** (1999) The variability of settling velocities of suspended fine-grained sediment in the ems estuary. *J. Sea Res.*, **41**, 109–118.
- Li, Z., Schieber, J. and Pedersen, P.K.** (2021) On the origin and significance of composite particles in mudstones: examples from the Cenomanian Dunvegan formation. *Sedimentology*, **68**, 737–754.
- Lick, W., Huang, H. and Jepsen, R.** (1993) Flocculation of fine-grained sediments due to differential settling. *J. Geophys. Res. Oceans*, **98**, 10279–10288.
- Macquaker, J.H.S. and Bohacs, K.M.** (2007) On the accumulation of mud. *Science*, **318**, 1734–1735.
- Manning, A.J. and Dyer, K.R.** (1999) A laboratory examination of floc characteristics with regard to turbulent shearing. *Mar. Geol.*, **160**, 147–170.
- McAnally, W.H. and Mehta, A.J.** (2002) Significance of aggregation of fine sediment particles in their deposition. *Estuar. Coast. Shelf Sci.*, **54**, 643–653.
- McCave, I.N.** (1975) Vertical flux of particles in the ocean. *Deep Sea Res. Oceanogr.*, **22**, 491–502.
- McCave, I.N. and Hall, I.R.** (2006) Size sorting in marine muds: processes, pitfalls, and prospects for paleoflow-speed proxies. *Geochem. Geophys. Geosyst.*, **7**, 1–37.
- McCool, W.W. and Parsons, J.D.** (2004) Sedimentation from buoyant fine-grained suspensions. *Cont. Shelf Res.*, **24**, 1129–1142.
- Mehta, A.J., Hayter, E.J., Parker, W.R., Krone, R.B. and Teeter, A.M.** (1989) Cohesive sediment transport. I: process description. *J. Hydraul. Eng.*, **115**, 1076–1093.
- Mehta, A.J. and Lott, J.W.** (1987) Sorting of fine sediment during deposition. In: *Coastal Sediments '87* (Ed Kraus, N.C.), pp. 348–362. American Society of Civil Engineers, New York, NY.
- Mehta, A.J. and Partheniades, E.** (1979) Kaolinite resuspension properties. *J. Hydraul. Eng.*, **105**, 411–416.
- Middleton, G.V. and Southard, J.B.** (1984) Mechanics of sediment movement. *SEPM Short Course*, **3**, 257.
- Mietta, F., Chassagne, C., Manning, A.J. and Winterwerp, J.C.** (2009) Influence of shear rate, organic matter content, pH and salinity on mud flocculation. *Ocean Dynamics*, **59**, 751–763.
- Milligan, T.G. and Hill, P.** (1998) A laboratory assessment of the relative importance of turbulence, particle composition, and concentration in limiting maximal floc size and settling behavior. *J. Sea Res.*, **39**, 227–241.
- Newport, L.P., Aplin, A.C., Gluyas, J.G., Greenwell, H.C. and Gröcke, D.R.** (2016) Geochemical and lithological controls on a potential shale reservoir: carboniferous Holywell shale, Wales. *Mar. Petrol. Geol.*, **71**, 198–210.
- Parham, W.E.** (1966) Lateral variations of clay mineral assemblages in modern and ancient sediments. *Proc. Int'l. Clay Conf.*, **1**, 135–145.
- Patterson, J.W.** (1985) *Industrial Wastewater Treatment Technology*, 2nd edn. Butterworth Publishers, Boston.
- Plint, A.G., Macquaker, J.H.S. and Varban, B.L.** (2012) Bedload transport of mud across a wide, storm-influenced ramp: Cenomanian-Turonian Kaskapau formation, Western Canada Foreland Basin. *J. Sed. Res.*, **82**, 801–822.
- Potter, P.E., Maynard, J.B. and Depetris, P.J.** (2005) *Mud and Mudstones*, p. 297. Springer Verlag, Berlin.
- Ross, M.A. and Mehta, A.J.** (1989) On the mechanics of lutoclines and fluid mud. *J. Coastal Res.*, **5**, 51–62.
- Safak, I., Allison, M.A. and Sheremet, A.** (2013) Floc variability under changing turbulent stresses and sediment availability on a wave energetic muddy shelf. *Cont. Shelf Res.*, **53**, 1–10.
- Schieber, J.** (2011) Reverse engineering mother nature – shale sedimentology from an experimental perspective. *Sed. Geol.*, **238**, 1–22.
- Schieber, J.** (2016) Mud-redistribution in epicontinental basins – exploring likely processes. *Marine Petrol. Geol.*, **71**, 119–133.
- Schieber, J., Miclaus, C., Seserman, A., Liu, B. and Teng, J.** (2019) When a mudstone was actually a “sand”: results of a sedimentological investigation of the bituminous marl formation (Oligocene), eastern Carpathians of Romania. *Sed. Geol.*, **384**, 12–28.
- Schieber, J. and Southard, J.B.** (2009) Bedload transport of mud by floccule ripples—direct observation of ripple migration processes and their implications. *Geology*, **37**, 483–486.
- Schieber, J., Southard, J.B., Kissling, P., Rossman, B. and Ginsburg, R.** (2013) Experimental deposition of carbonate mud from moving suspensions: importance of flocculation and implications for modern and ancient carbonate mud deposition. *J. Sed. Res.*, **83**, 1025–1031.
- Schieber, J., Southard, J. and Thaisen, K.** (2007) Accretion of mudstone beds from migrating floccule ripples. *Science*, **318**, 1760–1763.
- Schllichting, H.** (1979) *Boundary Layer Theory*, p. 817. McGraw-Hill, New York, NY.
- Schofield, R.K. and Samson, H.R.** (1954) Flocculation of kaolinite due to the attraction of oppositely charged crystal faces. *Discuss. Faraday Soc.*, **16**, 135–145.
- Shchepetkina, A., Gingras, M.K. and Pemberton, S.G.** (2018) Modern observations of floccule ripples: Petitcodiac River estuary, New Brunswick, Canada. *Sedimentology*, **65**, 582–596.
- Smith, L.B., Schieber, J. and Wilson, R.D.** (2019) Shallow-water onlap model for the deposition of Devonian black shales in New York, USA. *Geology*, **47**, 279–283.
- Sorby, H.C.** (1908) On the application of quantitative methods to the study of the structure and history of rocks. *Quart. J. Geol. Soc.*, **64**, 171–233.

- Steel, R.J. and Milliken, K.L.** (2013) Major advances in siliciclastic sedimentary geology, 1960–2012. In: *The Web of Geological Sciences: Advances, Impacts, and Interactions*. Geol. Soc. Am. Spec. Paper (Ed Bickford, M.E.), Vol. 500, pp. 121–167. Geological Society of America, Boulder, CO.
- Sternberg, R.W., Berhane, I. and Ogston, A.S.** (1999) Measurement of size and settling velocity of suspended aggregates on the northern California continental shelf. *Mar. Geol.*, **154**, 43–53.
- Stone, M. and Krishnappan, B.G.** (2003) Floc morphology and size distributions of cohesive sediment in steady-state flow. *Water Res.*, **37**, 2739–2747.
- Svititski, J.P.M., Asprey, K.W. and Leblanc, K.W.G.** (1995) In-situ characteristics of particles settling within a deep-water estuary. *Deep-Sea Res. II Top. Stud. Oceanogr.*, **42**, 223–256.
- Trabucho-Alexandre, J., Dirkx, R., Veld, H., Klaver, G. and de Boer, P.L.** (2012) Toarcian black shales in the Dutch central graben: record of energetic, variable depositional conditions during an oceanic anoxic event. *J. Sed. Res.*, **82**, 104–120.
- Tran, D. and Strom, K.** (2017) Suspended clays and silts: are they independent or dependent fractions when it comes to settling in a turbulent suspension? *Cont. Shelf Res.*, **138**, 81–94.
- Van Olphen, H.** (1977) *An Introduction to Clay Colloid Chemistry*, 2nd edn, p. 290. National Academy of Sciences, Washington, DC.
- Verwey, E.J.W. and Overbeek, J.T.G.** (1948) Theory of the stability of lyophobic colloids. *J. Phys. Colloid Chem.*, **51**, 631–636.
- van der Walt, S., Schönberger, J.L., Nunez-Iglesias, J., Boulogne, F., Warner, J.D., Yager, N., Gouillart, E., Yu, T. and The Scikit-Image Contributors** (2014) Scikit-image: image processing in python. *PeerJ*, **2**. <https://doi.org/10.7717/peerj.453>.
- Winterwerp, J.C. and van Kesteren, W.G.M.** (2004) *Introduction to the Physics of Cohesive Sediment Dynamics in the Marine Environment*, p. 466. Elsevier, Amsterdam.
- Xu, F., Wang, D.-P. and Riemer, N.** (2008) Modeling flocculation processes of fine-grained particles using a size-resolved method: comparison with published laboratory experiments. *Cont. Shelf Res.*, **28**, 2668–2677.
- Yawar, Z. and Schieber, J.** (2017) On the origin of silt laminae in laminated shales. *Sed. Geol.*, **360**, 22–34.
- Yawar, Z. and Schieber, J.** (2019) How Mud and Sand May Mingle: Exploring Co-Transport and Deposition Sand and Mud with Flume Experiments - Implications for Shale Sedimentology and Fluvial Systems. American Geophysical Union, Fall Meeting 2019, abstract #EP51E-2138.
- Ye, L., Manning, A.J. and Hsu, T.-J.** (2020) Oil-mineral flocculation and settling velocity in saline water. *Water Res.*, **173**, 115569.
- Zbik, M.S., Smart, R.S.C. and Morris, G.E.** (2008) Kaolinite flocculation structure. *J. Colloid Interf. Sci.*, **328**, 73–80.

Manuscript received 29 January 2022; revision accepted 1 August 2022

Supporting Information

Additional information may be found in the online version of this article:

Appendix S1. Reynolds Number for Rectangular Duct.

Appendix S2. X-ray diffraction (XRD) Data for Acti-Min SA1 kaolin, supplied by Active Minerals International LLC, Gordon, Georgia.